Chapter 5

Dynamics of Organocations Intercalated in Tetrasilicicfluormica

5.1 Results and Discussion

A. *n*-Octylammonium-Tetrasilicicfluormica (C81-MC and C81d_3-MC)

^{1}H NMR spectra

A temperature dependence of ^{1}H NMR spectra observed in C81-MC are shown in Figure 5.A.1. All spectra could be explained by superposition of two components consisting of a major broad and a minor sharp signal. The latter component could be observed even at 108 K, while the former was narrowed upon heating. These facts imply the existence of at least two kinds of *n*-octylammonium ions in different motional states, or in different circumstances. Applying a similar discussion to that in 4.1.A, the sharp component is assignable to movable ions located in spatially less-restricted positions where the interlayer distance is relatively long. By comparison of areas of sharp and broad spectrum components, the latter was shown to be major.

Second moment of ^1H NMR spectra

Figure 5.A.2 shows the temperature dependence of ^1H NMR M_2 observed in C81-MC. The M_2 of 16 ± 3 G^2 observed at ca. 100 K agreed with the calculated value of 15 G^2 for the model of the reorientation of NH_3^+ groups about its C_3 axis together with the C_3 rotation of CH_3 groups ([CH_3-rot]+[NH_3^+-rot]), implying that these rotational modes of the intercalated ions are excited below 100 K. With increasing temperature, M_2 was reduced gradually over a temperature range 150-450 K and M_2 of 4.4 G^2 obtained at 411 K corresponds to the theoretical value of 4.3 G^2 for the model of cationic uniaxial rotation around its long axis together with [CH_3-rot] and [NH_3^+-rot]. This result indicates that the occurrence of the uniaxial rotation above 150 K, but the temperature dependence of M_2 in this region cannot be explained by the motion characterized by the Arrhenius-type single correlation time.

^2H NMR spectra

The temperature dependence of ^2H NMR spectra in C81d_3-MC observed in a range 108-480 K is shown in Figure 5.A.3. The spectrum at 108 K exhibited a typical Pake pattern with a small asymmetry parameter, $\eta \leq 0.1$. A spectrum narrowing was observed with increasing temperature and, above 300 K, another spectral component appeared inside the broad component. Quadrupole coupling constants (QCC) of the broad component were estimated by the spectrum fitting, and its temperature dependence is shown in Figure 5.A.4. Calculation of QCC values was carried out for possible motional modes in the interlayer space, i.e., the reorientation of ND_3^+ group

about its C_3 axis [ND_3^+-rot], and the cationic uniaxial rotation as a whole about its long axis [uniaxial-rot]. In this calculation, we employed the QCC value of 173 kHz reported for rigid $C_2H_5ND_3Cl$ at 77 K [8], and assumed tetrahedral bond angles in the cation. The calculated values of 58 and 22 kHz for [ND_3^+-rot] and [uniaxial-rot], respectively, are shown in Fig. 5.A.4 by broken lines. The onset of the ND_3^+ reorientation is expected below 108 K because the observed QCC of 58 kHz is explainable by this motion. Over a wide temperature range of 150-440 K, the QCC value decreased very gradually and seemed to approach to the value calculated for uniaxial rotation. This unusually gradual QCC reduction, as is analogous to M_2 behavior, is attributable to onset of the uniaxial rotation taking place between asymmetric potential wells by following reasons: The first, it is impossible to introduce a large distribution in the motional correlation time, as shown in saponite compounds, because there is a little inhomogeniety in cationic circumstances from the consideration of the result of XRD analysis. The second, since the long and short diameters of an *n*-octylammonium ion are estimated to be ca. 4.5 and 4.2 Å, respectively, a model of asymmetric potential wells for two different orientations of a cation is acceptable as illustrated in Fig. 5.A.5, and this model can explain the gradual reduction of QCC. Above 460 K, the linewidth of the outer component in ^2H NMR spectra was narrowed to less than ca. 5 kHz. This indicates the excitation of another motion such as the whole ionic rotation around the axis perpendicular to the molecular axis, because only this mode can reduce the linewidth to the observed value with negligible expansion of the interlayer space.

^1H NMR spin-lattice relaxation times (T_1)

^{1}H NMR T_1 values measured in C81-MC at 48.9 and 25.6 MHz, and C81d_3-MC at 48.9 MHz are plotted in Figure 5.A.6. A frequency dependent T_1 was observed in C81-MC in a range 89-400 K, indicating the presence of magnetic dipolar relaxation processes. T_1 in C81-MC observed at 48.9 MHz showed a broad and a sharp minimum at *ca.* 130 and 300 K, respectively. In the range 89-200 K, T_1 in C81d_3-MC was longer than that in C81-MC, while these T_1 values became close with each other above 200 K.

The T_1 data in C8-MC observed below 200 K can be expressed by the superposition of two BPP-type relaxation rate given by

$$T_1^{-1} = \sum_{i=1}^{2} T_{1i}^{BPP} \qquad (7),$$

each of which is expressed as [10]

$$\frac{1}{T_1^{BPP}} = \frac{2}{3}\gamma^2 \Delta M_2 \left\{ \frac{\tau}{1+\omega_0^2\tau^2} + \frac{4\tau}{1+4\omega_0^2\tau^2} \right\} \qquad (8)$$

where γ, ΔM_2, and ω_0 are the gyromagnetic ratio of a proton, the difference in the second moment of the ^{1}H NMR linewidth before and after the onset of the motion, and the angular Larmor frequency of a proton, respectively. We assume an Arrhenius-type relationship between the correlation time τ and temperature T with the activation energy E_a of the motion written as

$$\tau = \tau_\infty \exp\left(\frac{E_a}{RT}\right) \qquad (9)$$

where τ is the correlation time in the limit of infinite temperature. Referring to the ^{2}H QCC analysis given above, the T_1 minimum observed at 300 K can be attributed to the reorientation of *n*-octylammonium ions about its long axis in unequal potential wells

from the following two reasons. The one is that, in the temperature range where the T_1 minimum was observed, ^{2}H QCC in C81d_3-MC is still in the process of narrowing and not narrowed completely to the theoretical value for this uniaxial rotation. This unusual QCC variation contradicts the consideration of a single excitation process in which motional time scales for the spectrum narrowing and the T_1 minimum are quite different. As the other reason, ΔM_2 of 6 G^2 derived from the T_1 value of 72 ms at the minimum observed at 48.9 MHz is too small compared with 10.5 G^2 calculated for the cationic uniaxial reorientation between the equivalent potential wells. This is because the increase of the T_1 minimum value is expected for motions in the asymmetric potential well as discussed below. In the range above 250 K, it is assumed that cations experience four equilibrium orientations obtainable by successive 90° rotations about the long axis as illustrated in Figure 5.A.5. These four positions are labeled in turn by **1**, **2**, **1** and **2** where the potential depths at **1** and **1** or **2** and **2** can be regarded as almost the same. Activation barriers from positions **1** and **2** are expressed as E_{a1} and E_{a2} ($E_{a1}>E_{a2}$), respectively, as shown in Fig. 5.A.5. The theoretical T_1 curve for this asymmetric potential model is given by [16]

$$\frac{1}{T_1^{ASYM}} = \frac{2}{3}\gamma^2\Delta M_2\left\{\frac{4\varepsilon}{(1+\varepsilon)^2}\right\}\left\{\frac{\tau}{1+\omega_0^2\tau^2}+\frac{4\tau}{1+4\omega_0^2\tau^2}\right\} \tag{10}$$

$$\varepsilon = \exp\left(\frac{E_{a1}-E_{a2}}{RT}\right) \tag{11}$$

$$\tau = \tau_\infty\left(\frac{2}{1+\varepsilon}\right)\exp\left(\frac{E_{a1}}{RT}\right) \tag{12}$$

The total T_1 value is given by the sum of Eqs. (7) and (10). The best fitted T_1 curves and determined motional parameters are shown in Fig. 5.A.6 and Table 5.A.1, respectively.

The asymmetric potential model is acceptable in this system because ΔM_2 of 11 ± 2 G^2 derived from the minimum observed at 300 K agrees with the value of 10.5 G^2 calculated for the uniaxial rotation. From the ^2H QCC analysis, it was shown that the NH_3^+ reorientation occurs below ca. 100 K. We can reasonably assign the minimum observed around 100 K to the NH_3^+ reorientation about the C_3 axis, because the observed T_1 in C81d_3-MC in this temperature range is much longer than T_1 in C81-MC, as is explainable by the effect of the NH_3^+ deuteration. The fact that the ΔM_2 of 2.9 G^2 obtained for the C_3 rotation of NH_3^+ was smaller than 3.7 G^2 calculated for this motion indicates that the motional correlation time seems to be somewhat distributed because of the heterogeneous circumstance made by the charge distribution in clay sheets of mica. The other T_1 minimum observed at ca. 150 K seems to be attributed to tumbling motions of the CH_3 ends in the layer plane with the fixed NH_3^+ ends. This is because ^2H QCC showed only NH_3^+ reorientation below this T_1 minimum temperature. In the temperature range up to 410 K, we could observed no T_1 decrease corresponding to the narrowed ^2H spectrum observed at 480 K, presumably because T_1 due to the in-plane tumbling of the whole cation giving the ^2H spectrum narrowing is too long to be detected below 410 K.

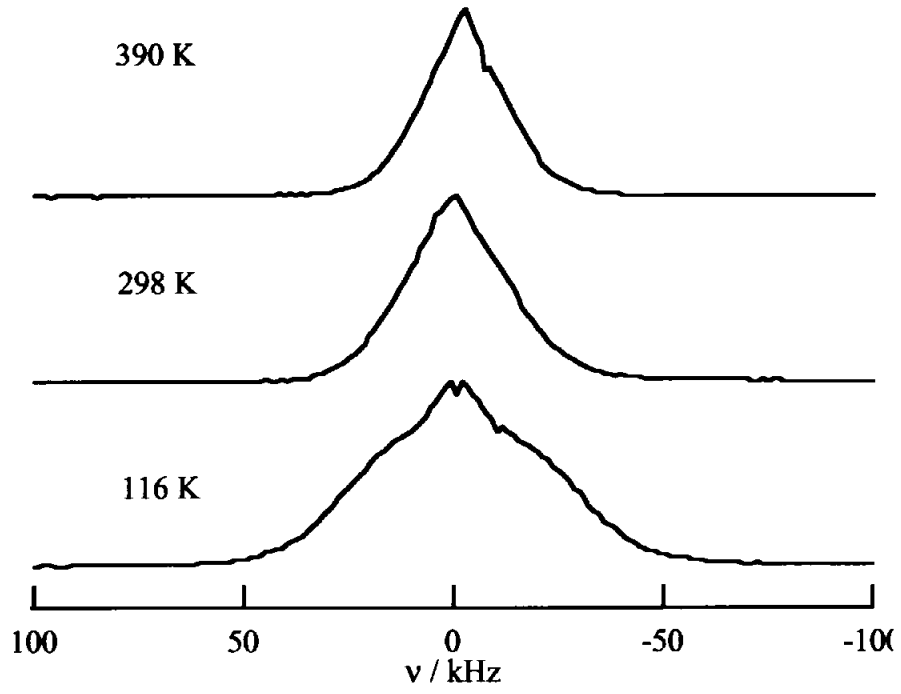

Fig. 5.A.1. ^{1}H NMR spectra observed in $CH_3(CH_2)_7NH_3$-tetrasilicicfluormica.

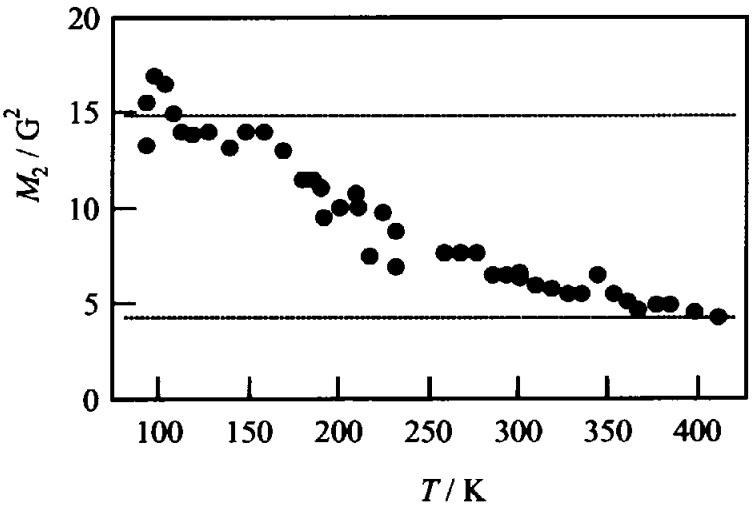

Fig. 5.A.2. ^{1}H NMR second moments (M_2) determined in $CH_3(CH_2)_7NH_3$-tetrasilicicfluormica. Dotted lines denote M_2 values calculated for the onset of CH_3 and NH_3^+ rotations about their C_3 axes ([CH_3-rot]+[NH_3-rot], upper) and the excitation of the cationic uniaxial rotation as a whole about its long axis together with [CH_3-rot]+[NH_3-rot](lower).

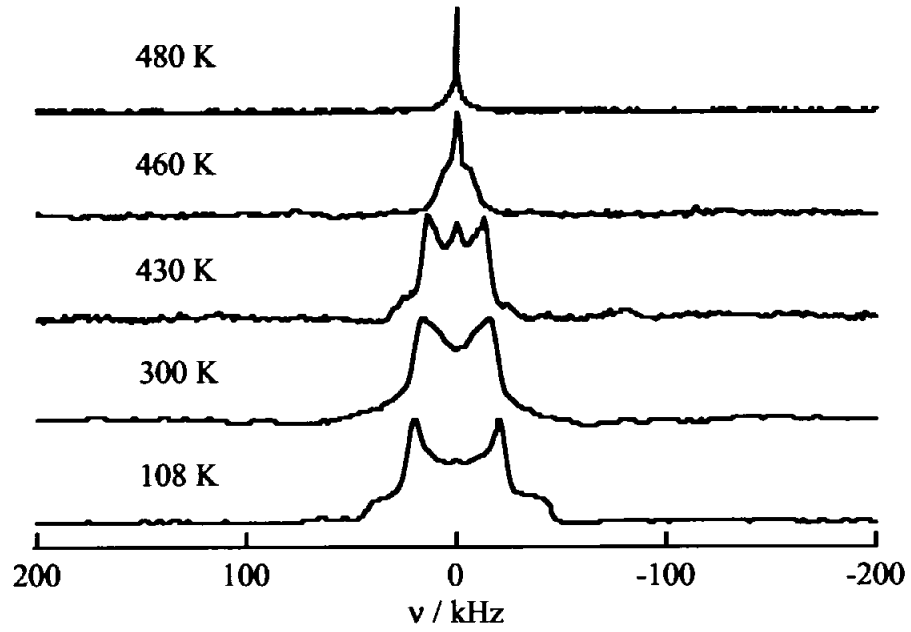

Fig. 5.A.3. ^{2}H NMR spectra observed in $CH_3(CH_2)_7ND_3$-tetrasilicicfluormica.

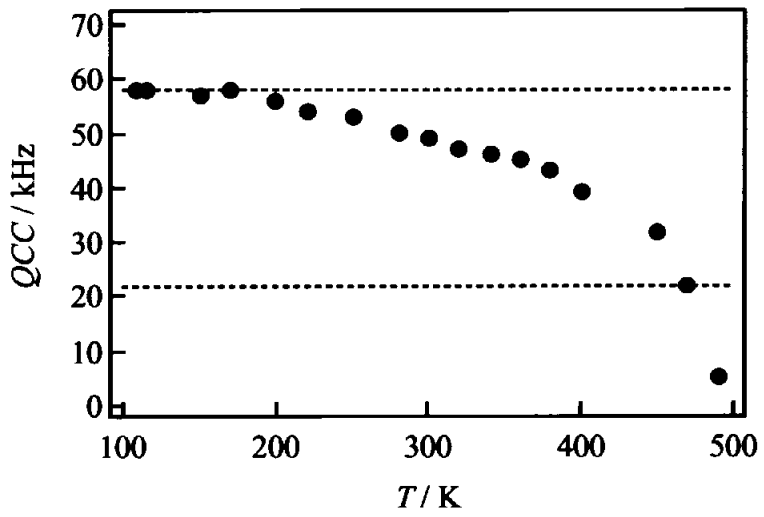

Fig. 5.A.4. The temperature dependence of quadrupole coupling constants (QCC) estimated from the linewidths of ^{2}H NMR spectra observed in $CH_3(CH_2)_7ND_3$-tetrasilicicfluormica. Broken lines stand for the calculated QCC for the motional modes of $CH_3(CH_2)_7ND_3^+$ ion: ND_3^+ rotation about its C_3 axis (upper) and the uniaxial rotation as a whole about its long axis (lower).

(a)

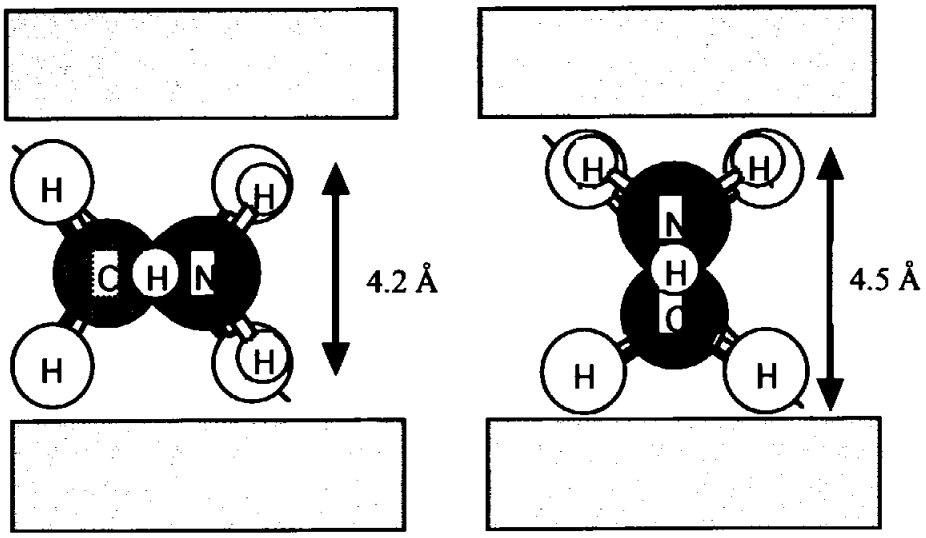

1 2

(b)

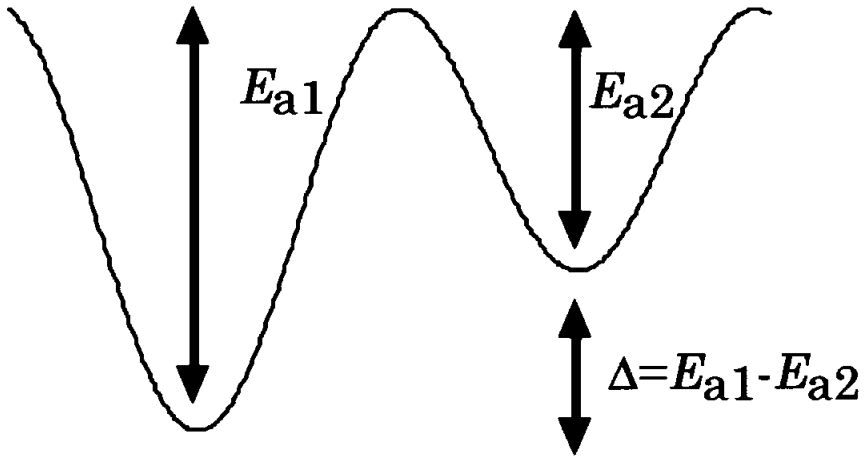

Fig. 5.A.5. (a) Two non-equivalent orientations (1 and 2) of an n-$C_8H_{17}NH_3^+$ ion in the interlayer space. (b)The asymmetric potential model for two non-equivalent orientations with activation energies of E_{a1} and E_{a2} for the n-$C_8H_{17}NH_3^+$ reorientation.

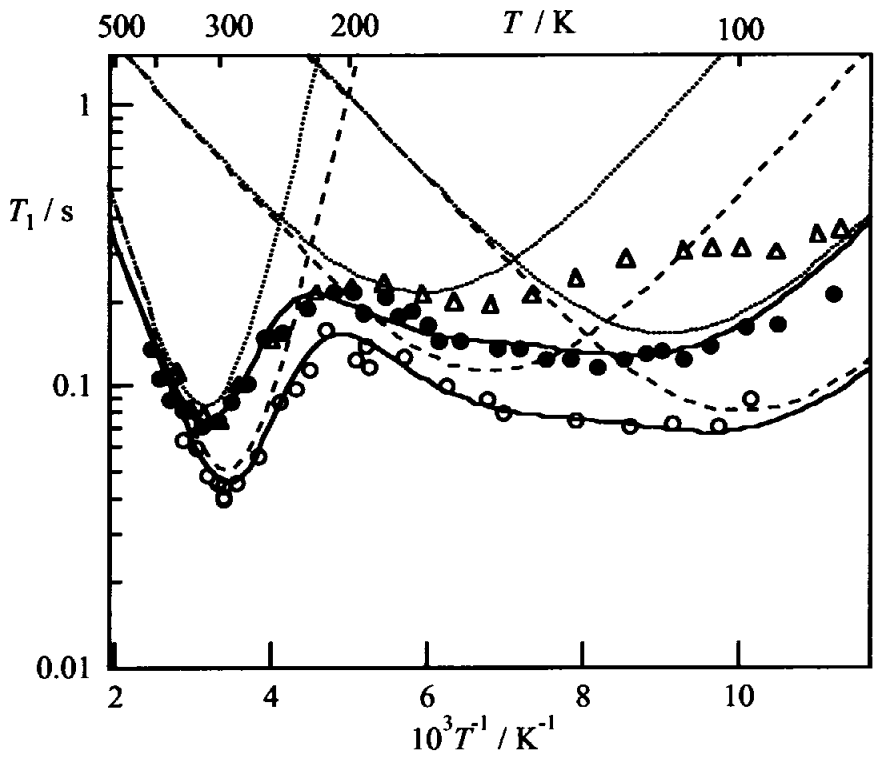

Fig. 5.A.6 ^1H NMR spin-lattice relaxation times T_1 observed at 48.9 MHz (●) and 25.6 MHz (○) in $CH_3(CH_2)_7NH_3$-tetrasilicicfluormica, and at 48.9 MHz (△) in $CH_3(CH_2)_7ND_3$-tetrasilicicfluormica. The dotted and broken lines denote calculated T_1 values at each frequency.

Table. 5.A.1. Motional modes, activation energies (E_a or $*E_{a1}$), reductions of second moments (ΔM_2) and a difference of potential depths ($*\Delta=E_{a1}-E_{a2}$) derived from ^1H NMR spin-lattice relaxation times observed in $CH_3(CH_2)_8NH_3$-tetrasilicicfluormica. Calculated ΔM_2 values are shown in parentheses. *: in the case of the asymmetric potential model.

motional mode	E_a ($*E_{a1}$) / kJ mol^{-1}	ΔM_2 /G^2	Δ / kJ mol^{-1}
NH_3^+-rot	5.5	2.9 (3.7)	-
CH_3-tumbling	5.9	2.1	-
uniaxial-rot	*23	*11(11)	*5.0

B. Octamethylenediammonium-Tetrasilicicfluormica (C82-MC and C82d_6-MC)

^{2}H NMR spectra

^{2}H NMR spectra observed in C82d_6-MC are shown in Figure 5.B.1. Spectra obtained below 450 K could be explained by the typical Pake pattern and their linewidths were narrowed very slowly with rising temperatures. At 470 K, the spectral pattern changed and above 470 K the linewidth was decreased steeply. The quadrupole coupling constants (QCC) determined from spectral linewidths are shown in Figure 5.B.2. Since QCC of 58 kHz observed at 145 K accords with that calculated for the NH_3^+ rotation about the C_3 axis, this motional mode is already excited below 145 K. In the range 150 to 250 K, the almost constant QCC value was obtained, and in 250 to 440 K a gradual QCC reduction was observed. At 470K, QCC became smaller than 22 kHz which was estimated for the uniaxial rotation as a whole cation around its long axis. From the analogy to the QCC analysis in C81d_3-MC, therefore, it is provable that the cationic uniaxial rotation in asymmetric potential wells occurs above 250 K.

^{1}H NMR spin-lattice relaxation time (T_1)

Temperature dependences of ^{1}H NMR T_1 observed in C82-MC at 54.3 and 25.7 MHz are shown in Figure 5.B.3. A minimum-like T_1 decrease could be seen around 100 K, and a steep reduction was observed at temperatures above 300 K. By referring to ^{1}H T_1 analysis in C81-MC and the result of QCC, it is likely that the minimum around 100 K is attributable to the NH_3^+ rotation about its C_3-axis [NH_3^+-rot]. The T_1 minimum

values observed around 100 K were 0.14 s at 54.3 MHz and 0.081 s at 25.7 MHz. These values are longer than the caluculated values of 0.086 s at 54.3 MHz and 0.041 at 25.7 MHz, respectively in case of the onset of C_3 rotation in both NH_3^+ terminal groups. Since it was predicted in C81-MC that the motional correlation time of NH_3^+ groups is distributed in this mode, those in C82-MC can be likewise. Taking into account the above discussion, T_1 curves in Fig. 5.B.3 were reproduced by a superposition of three theoretical T_1 curves: one in the low temperature range below 200 K was calculated by introducing distribution in the correlation time, which is expressed by Eqs. (3)-(5), and the other two are normal BPP type theoretical curves written by Eqs. (8) and (9). Each of fitted curves is given by a dotted line at 54.3 MHz or a broken line at 25.7 MHz, and the superpositions of these contributions are depicted by solid lines in Figure 5.B.3. Fitting parameters used in this optimization are tabulated in Table 5.B.1. Since T_1 variation between 100 and 200 K was well fitted by the theoretical curve with a large extent of distribution in the correlation time given by β=0.3, and the estimated ΔM_2 value of 6.3 G^2 is approximately equal to 5.8 G^2 calculated for excitation of NH_3^+-rot, the observed minimum is attributable to this mode and the circumstance of ammonium groups in C82-MC is highly inhomogeneous. The shallow T_1 minimum observed around 250 K can be assigned to a fluctuational motion of alkyl chains, because no QCC reduction observed between 150 and 250 K shown in Fig. 5.B.2 indicates that the direction of C_3 axis in ammonium groups is fixed in the interlayer space in this temperature region. Although it is conceivable that the T_1 decrease above 300 K is attributed to the uniaxial rotation of the octamethylenediammonium ions in the

asymmetric potential wells, which corresponds to the gradual QCC reduction above 250 K, detailed discussion cannot be done at this point since the corresponding T_1 minimum could not be observed.

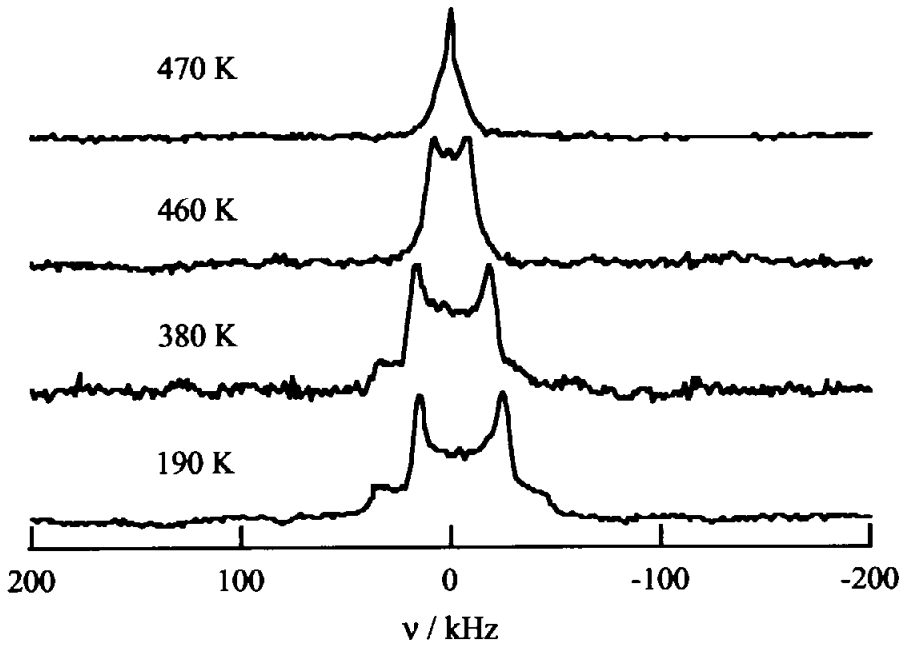

Fig. 5.B.1. ^{2}H NMR spectra observed in $ND_3(CH_2)_8ND_3$-tetrasilicicfluormica

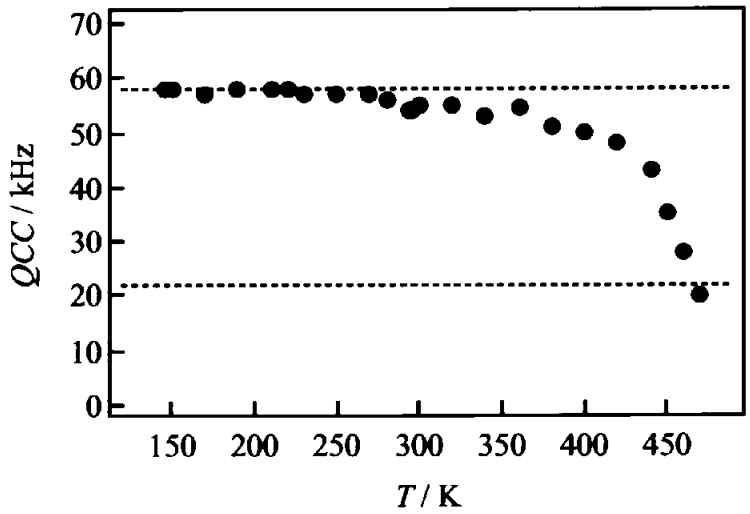

Fig. 5.B.2. The temperature dependence of quadrupole coupling constants (QCC) evaluated from the linewidths of ^{2}H NMR spectra observed in $ND_3(CH_2)_8ND_3$-tetrasilicicfluormica. Broken lines stand for the calculated QCC for the motional modes of $ND_3^+(CH_2)_8ND_3^+$ ion: ND_3^+ group s rotation about their C_3 axes (upper) and cationic uniaxial rotation as a whole about its long axis (lower).

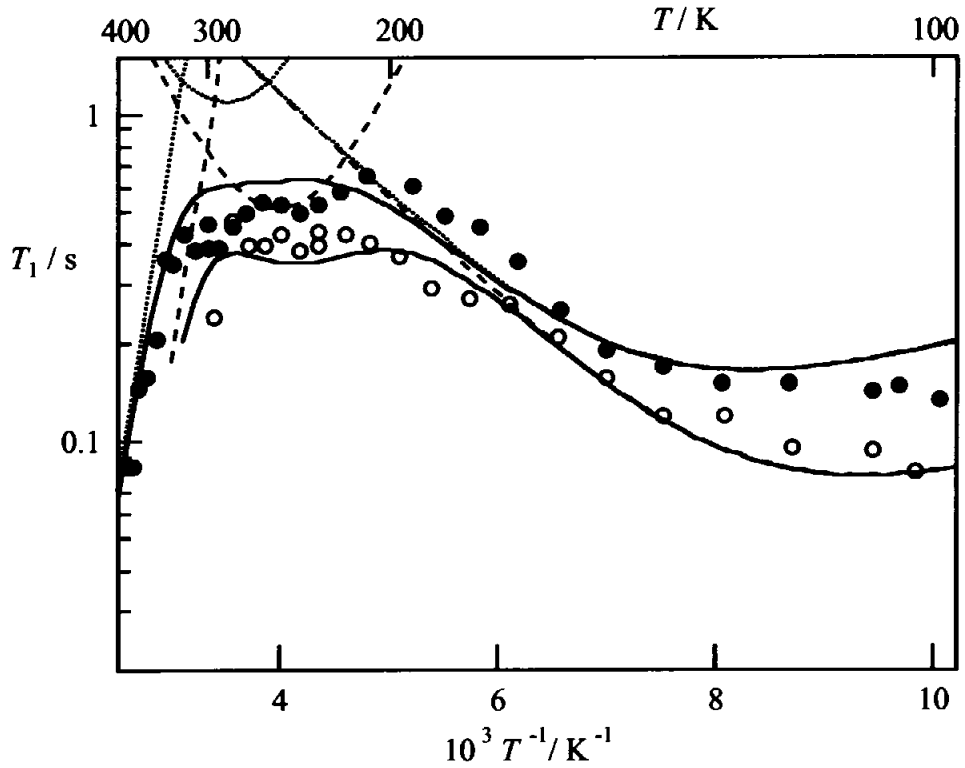

Fig. 5.B.3. ^{1}H NMR spin-lattice relaxation times T_1 observed at 54.3 MHz (●) and 25.7 MHz (○) in $NH_3(CH_2)_8NH_3$-tetrasilicicfluormica. Dotted and broken lines are respective T_1 components calculated at 54.3 and 25.7 MHz and these superpositions are expressed by solid lines.

Table 5.B.1. The fitting parameters for ^{1}H NMR spin-lattice relaxation times observed in $NH_3(CH_2)_8NH_3$-tetrasilicicfluormica: motional modes, activation energies (E_a), reductions of second moment (ΔM_2) and parameters presenting width of τ distribution (β). Calculated ΔM_2 values are shown in parenthesis.

motional mode	E_a / kJ mol^{-1}	ΔM_2	β
NH_3^+-rot	6.0	6.3	0.30
chain-fluctuation	13	0.50	-
uniaxial-rot	40	-	-

C. *n*-Butylammonium-Tetrasilicicfluormica (C41-MC and C41d_3-MC)

^{2}H NMR spectra

Temperature dependences of ^{2}H NMR spectra in C41d_3-MC and quadrupole coupling constants (QCC) estimated from these resonance linewidths are shown in Figure 5.C.1 and 5.C.2, respectively. The linewidth of ^{2}H NMR spectra decreased gradually on heating from 125 to 450 K. At 480 K, the linewidth decreased steeply, and a sharp component appeared at the center. Because the QCC value of 56 kHz observed at 125 K almost agrees with 58 kHz calculated for the model of the ND_3^+ rotation around its C_3 axis [ND_3^+-rot], it is probable that this mode is already excited below 125 K. Since a very gradual QCC decrease in a temperature range 140-450 K is similar to the phenomenon observed in C81-MC, it is likely that the cationic uniaxial rotation as a whole about its long axis is excited over a wide range of 350 K. From the analogy to the QCC analysis in C81d_3-MC, it is expected that a model of asymmetric potential wells for two different orientations of a cation can be adapted to the uniaxial rotation of *n*-butylammonium ions..

^{1}H NMR spin-lattice relaxation time (T_1)

Signal intensities ($M(\infty)$-$M(\tau)$) / $M(\infty)$ of recoveries of ^{1}H magnetization observed in C41-MC after a 180°-τ-90° pulses are shown in Figure 5.C.3. At 104 K, the almost whole part of recovery curves could be fitted by a single exponential curve. At temperatures higher than 290 K, recovery curves could be separated to two T_1

components: The best fitted slow-relaxing (long T_1) component was drawn by a solid line and the fast-relaxing (short T_1) one was by open circles, which is given by subtracting the contribution of the long T_1 component from the whole magnetization shown in Figure 5.C.3.

Figure 5.C.4 shows a temperature dependence of the ratio of the short T_1 component to the whole magnetization. The fraction of the short component was about 20 % in the low temperature region below 240 K, and increased above 270 K, and became more than 50 % in the high temperature range above 300 K.

Temperature dependences of ^{1}H NMR spin-lattice relaxation times observed in C41-MC at Larmor frequencies of 54.3 and 25.7 MHz and in C41d_3-MC at 54.3 MHz are shown in Figure 5.C.5. The short T_1 component observed in the temperature region above 300 K is also exhibited in Figure 5.C.5. A shallow T_1 minimum could be observed around 150 K at respective frequencies. This minimum can be decomposed into two minima by considering the frequency dependence and the T_1 values in C41d_3-MC in this temperature range. T_1 values observed in C41d_3-MC were longer than those in C41-MC around 100 K. From the analogy to the T_1 analysis in C81-MC, the T_1 behavior around 100 K can be attributed to the rotation of a NH_3^+ group about its C_3 axis. It is also conceivable that the T_1 variation around 180 K is assigned to tumbling motions of CH_3 ends. Although T_1 was reduced monotonically above 250 K, the observed frequency dependence became smaller than ω^2 above 300 K. T_1 values of the fast-relaxing component was also decreased with the rise of temperature, and they reached a few ms around 400 K. In the QCC analysis, it was predicted that the cationic uniaxial rotation is

excited at temperatures above 140 K. Hence, the T_1 reduction observed above 250 K is likely to be assigned to this mode, but even the long T_1 values of the slow-relaxing component, 12.5 ms at 54.3 MHz and 5.6 ms at 25.6 MHz observed at 400 K are too short to be explained by the onset of this motion through averaging of ^{1}H-^{1}H interaction, because the minimum T_1 values calculated for the uniaxial rotation mode are 48 ms at 54.3 MHz and 23 ms at 25.6 MHz. Judging from the frequency dependence of T_1 curves, it is feasible that the minimum caused by the uniaxial rotation is found in the temperature region around 300 K. T_1 values around 300 K are, however, long for minimum values derived from the uniaxial rotation. This disagreement can be explained by assuming the asymmetric potential model for this mode as mentioned in the QCC analysis.

In many cases, ^{1}H T_1 values less than a few ms can be explained by the interaction between ^{1}H spins and unpaired electron spins [10]. To confirm the presence of unpaired electrons, the ESR measurement was carried out. Derivative curves of ESR spectra in Na-MC observed at 300 K are shown in Figure 5.C.6. Two ESR signals with g factors of 2.0 and 4.4 were obtained in Na-MC, indicating the existence of electron spins in Na-MC. The signal with g=2.0 is assigned to paramagnetic Fe^{3+} ions substituting for Mg^{2+} sites inside the clay sheets, and the other with g=4.4 can be associated with spins of isolated Fe^{3+} ions [17]. By comparison of spectrum areas of both signals, it is revealed that electron spins mainly come from the former Fe^{3+} ions. By the X-ray fluorescence analysis it is ascertained that Na-MC contains Fe by 0.16 wt %, which corresponds to a Fe atom per the interlayer space of 50 Å^2, where

approximately 50 *n*-butylammonium ions are intercalated. Therefore, The T_1 decrease observed above 300 K is possibly explained by the interaction between ^{1}H spins and paramagnetic electron spins. Moreover, this T_1 behavior can be related with the cationic motion, because frequency dependences were observed above 300 K in both short and long T_1 components. By taking into consideration of the fact that no remarkable change could be observed in the ^{2}H spectral linewidth and its shape in the temperature range 140-450 K, cationic diffusion, which hardly affects the ^{2}H spectra, is expected to be excited. Now, the author suggests the following mechanism to account for the anomalously short T_1 values observed in C41-MC: In the high temperature region, the self-diffusion of *n*-butylammonium ions is excited in the two-dimensional space (2D diffusion), and distances (R) between electron spins (S) on paramagnetic Fe^{3+} sites and ^{1}H spins (I) of a cation vary with the cationic motion. If ^{1}H-electron dipolar interactions expressed as $\mathcal{H}_{IS} \cong \frac{\gamma_I \gamma_S \hbar}{R^3}$ fluctuate at the diffusional frequency of intercalated cations, spin-lattice relaxation of protons of *n*-butylammonium ions becomes effective. In such a case, T_1 is given by Solomon s equation [18],

$$\frac{1}{T_1^{\mathrm{PARA}}} = C\left\{\frac{\tau}{1+(\omega_I-\omega_S)^2\tau^2} + \frac{\tau}{1+\omega_I^2\tau^2} + \frac{\tau}{1+(\omega_I+\omega_S)^2\tau^2}\right\} \qquad (13)$$

where C, τ, ω_I (ω_s) are the motional parameter, the diffusional correlation time of the cation, and the Larmor frequency of a proton (electron), respectively. The motional constant C is connected with R by the following expression,

$$C \propto \frac{\gamma_I^2 \gamma_S^2 \hbar^2}{\langle R^6 \rangle_{av}} \qquad (14).$$

From the combination of Eq. (13) and (14), it is readily found that short R gives short T_1.

It is likely that two T_1 components observed in the high temperature region are assigned to two groups of intercalated cations: one diffuses in the vicinity of paramagnetic sites, the other does in the region apart from paramagnetic sites. The increase of the fraction in the short T_1 component upon heating (see Fig. 5.C.4) means that the number of intercalated ions which can diffuse widely and come close to the paramagnetic site increases with the rise of temperature. The total T_1 curve of the slow-relaxing component was fitted by the superposition of four calculated T_1 curves given by

$$\frac{1}{T_1} = \sum_{i=1}^{2} \frac{1}{T_{1i}^{\mathrm{BPP}}} + \frac{1}{T_1^{\mathrm{ASYM}}} + \frac{1}{T_1^{\mathrm{PARA}}}. \qquad (15)$$

Each T_1 curve calculated at 54.3 or 25.6 MHz is depicted by a dotted or a broken line, and the total T_1 curves are by solid lines in Figure 5.C.5. T_1 values of the fast-relaxing component were also fitted by using Eq. (13), and shown in Figure 5.C.7. Obtained motional parameters are shown in Table 5.C.1.

Electrical Conductivity

The ac electric conductivity σ could be measured in C41-MC at 1kHz in the temperature region above 300 K. On heating the specimen, the conductivity increased from values of the order of 10^{-5} to 10^{-4} S m^{-1}. The σT plots are shown in Figure 5.C.8. The closed circles denote the values obtained by the first measurement in the virgin sample, and open circles by the second run in the same sample. In both the first and the second measurements, σT increased linearly with the temperature, and σT values obtained in both measurements were approximately same within experimental errors.

The linear increase of σT indicates the presence of ionic conduction. Accordingly, the onset of 2D diffusion of *n*-butylammonium ions was confirmed. Activation energies (E_a) of the 2D diffusion of *n*-butylammonium ions can be determined from slopes of $\ln(\sigma T)$ vs. T^{-1} plots by using the Nernst-Einstein relation. The obtained activation energies in the first run is 27±1 and 28±1 kJ mol^{-1} in the second run is. These values are comparable to 18 and 22 kJ mol^{-1} determined in ^1H T_1 analysis.

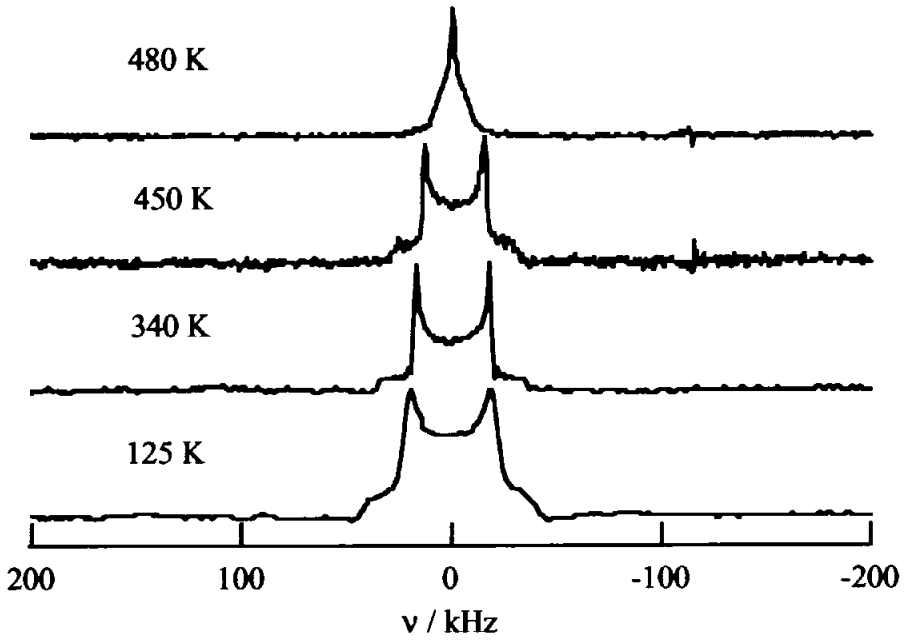

Fig. 5.C.1. ^{2}H NMR spectra observed in $CH_3(CH_2)_3ND_3$-tetrasilicicfluormica.

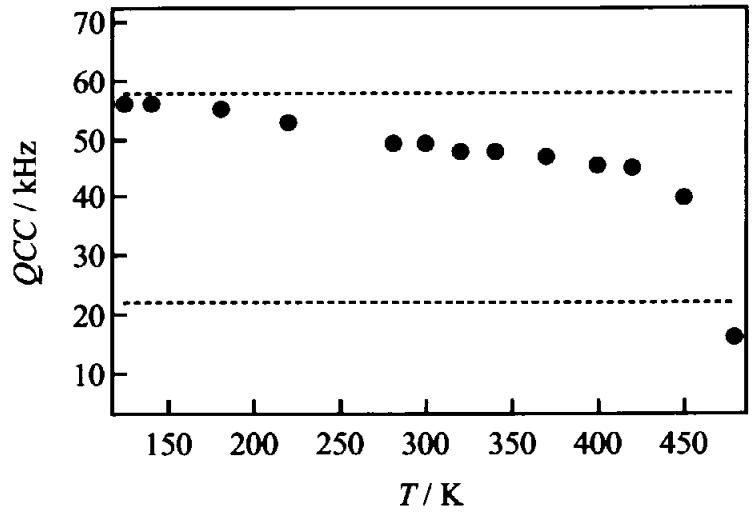

Fig. 5.C.2. The temperature dependence of quadrupole coupling constants (QCC) estimated from linewidths of ^{2}H NMR spectra observed in $CH_3(CH_2)_3ND_3$-tetrasilicicfluormica. Broken lines stand for the calculated QCC for motional modes of $CH_3(CH_2)_3ND_3^+$ ion: ND_3^+ rotation about its C_3 axis (upper) and cationic uniaxial rotation as a whole about its long axis (lower).

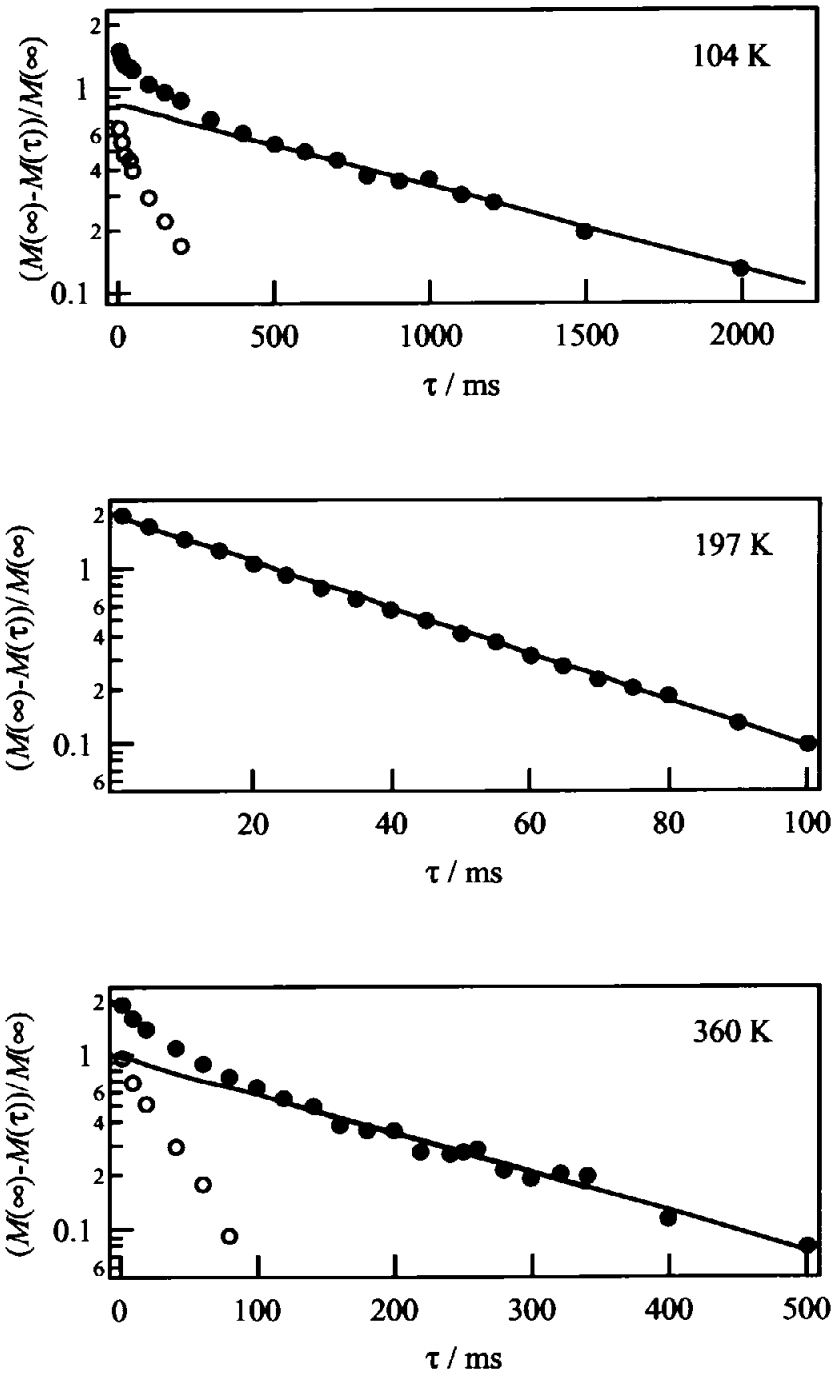

Fig. 5.C.3 Recoveries of ^{1}H magnetization (●) observed at a Larmor frequency of 54.3 MHz in $CH_3(CH_2)_3NH_3$-tetrasilicicfluormica. The slope of solid line affords the spin-lattice relaxation time (T_1) of the slow-relaxing component. The fast-relaxing component (○) is give by the difference between the observed magnetization and the solid line.

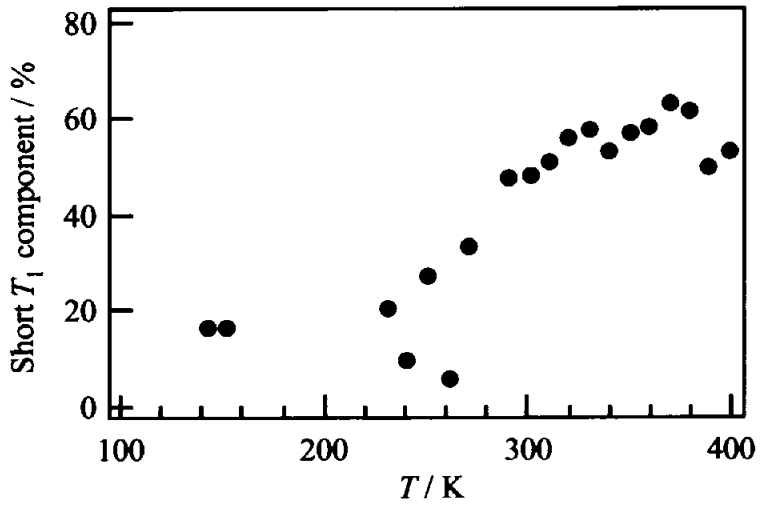

Fig. 5.C.4. The temperature dependence of the short T_1 component observed in C41-SP.

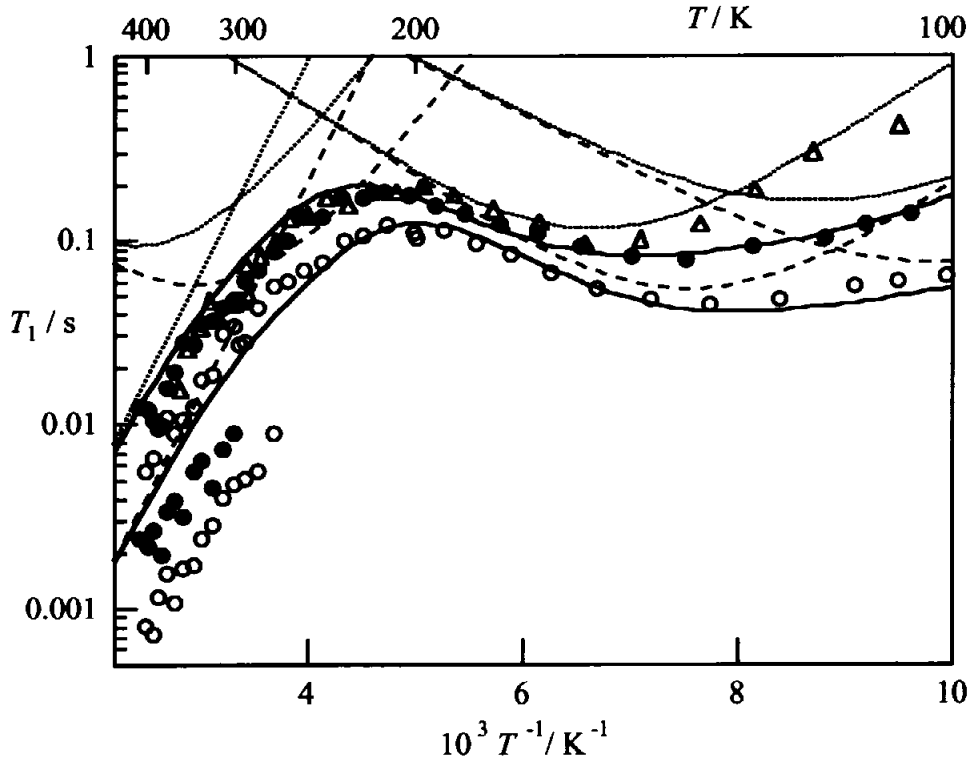

Fig. 5.C.5. ^1H NMR spin-lattice relaxation times T_1 observed at 54.3 MHz (●) and 25.7 MHz (○) in $CH_3(CH_2)_3NH_3$-tetrasilicicfluormica, and at 54.3 MHz (△) in $CH_3(CH_2)_3ND_3$-tetrasilicicfluormica. Dotted and broken lines are respective T_1 components calculated at 54.3 and 25.7 MHz, and their superpositions are expressed by solid lines.

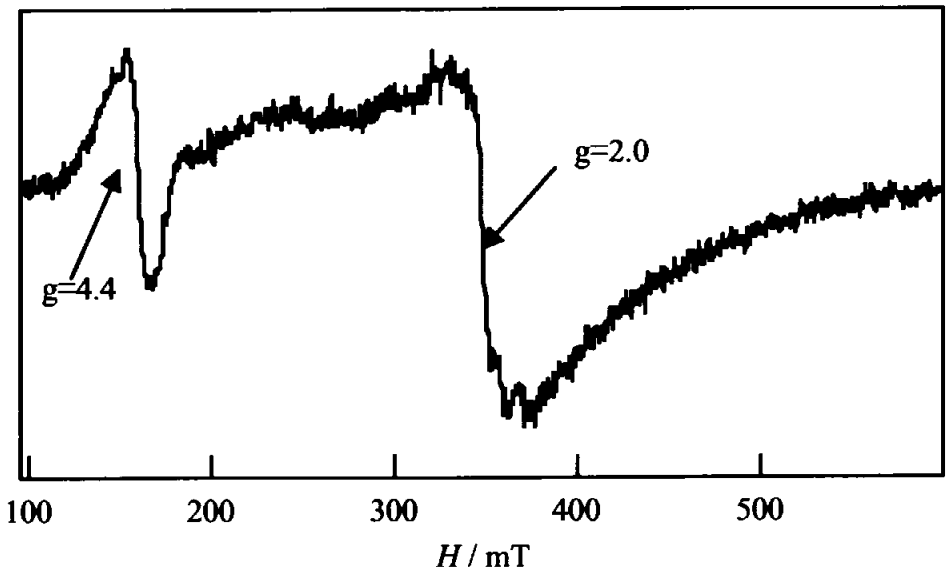

Fig. 5.C.6. The derivative spectrum of electron spin resonance spectra observed in Na-tetrasilicicfluormica at 300 K.

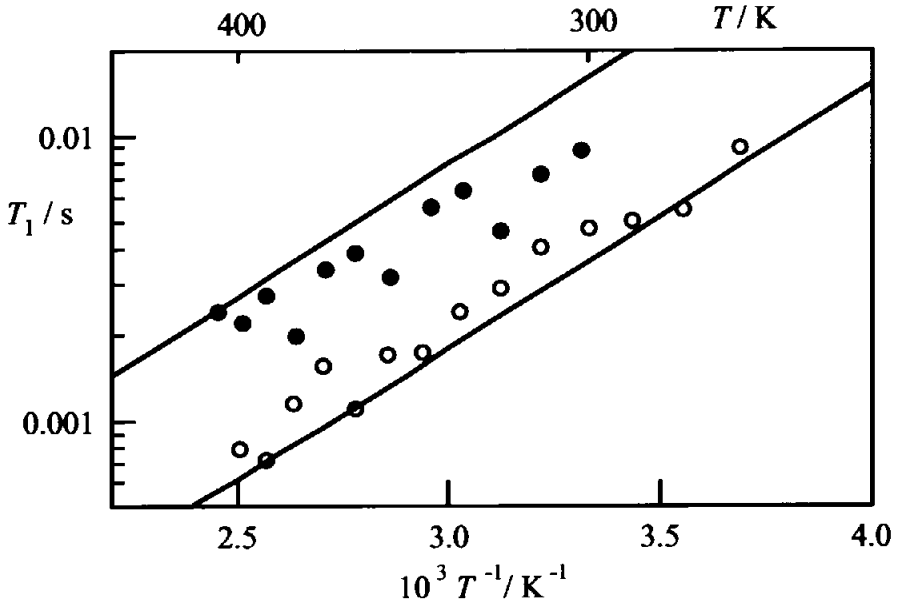

Fig. 5.C.7. The temperature dependence of the short T_1 component observed at 54.3 (●) and 25.7 MHz (○). Solid lines denote T_1 values calculated by considering paramagnetic interactions.

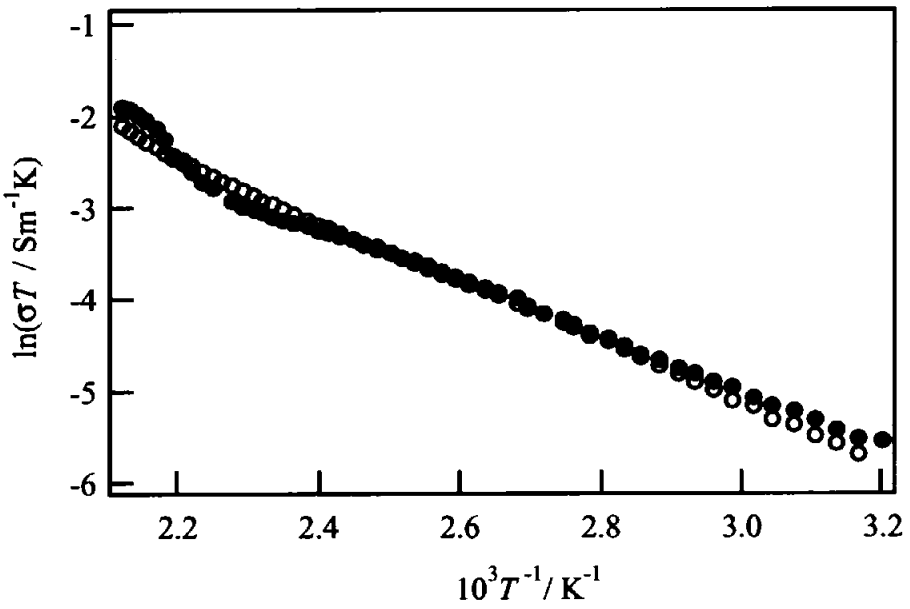

Fig. 5.C.8. The temperature dependence of ac electrical conductivity σ observed in $CH_3(CH_2)_3NH_3$-tetrasilicicfluormica by the two-terminal method at 1 kHz. Closed and open circles stand for the values obtained in the virgin sample and that once heated, respectively.

Table 5.C.1. Fitting parameters of ^1H NMR spin-lattice relaxation times observed in $CH_3(CH_2)_3NH_3$-tetrasilicicfluormica: motional modes, activation energies (E_a or $*E_{a1}$), reductions of second moment (ΔM_2) and a difference of asymmetric potential depths ($\Delta=E_{a1}-E_{a2}$). Calculated values of ΔM_2 are shown in parentheses. *: the case of asymmetric potential model.

motional mode	E_a ($*E_{a1}$) / kJ mol^{-1}	ΔM_2 / G^2	$*\Delta$ / kJ mol^{-1}
CH_3-rot	5.7	3.1(3.6)	-
NH_3^+-rot	7.1	4.3(5.4)	-
uniaxial-rot	*14	*9.1(11)	*5.0
2D-diffusion	18 (short) 22 (long)	-	-

D. Tetramethylenediammonium-Tetrasilicicfluormica (C42-MC and C42d_6-MC)

^2H NMR spectra

^{2}H NMR spectra observed in C42d_6-MC are shown in Figure 5.D.1, The spectrum obtained at 140 K gave a typical Pake pattern. At temperatures above 220 K, the spectrum linewidth was reduced gradually. At 400 K, a very narrowed component appeared, and its intensity was increased with temperature. Quadrupole coupling constants (QCC) estimated from the linewidths of the wide spectrum component are shown in Figure 5.D.2. Since the QCC of 56 kHz obtained in the temperature region of 140-200 K agrees with 58 kHz calculated for the ND_3^+ rotation around their C_3 axis, this mode for both ND_3^+ groups is already excited below 140 K. The gradual QCC reduction was seen in a temperature range 220-440 K, and its value approached to 22 kHz calculated for the cationic uniaxial rotation as a whole about its long axis. By referring to the QCC analysis in C81d_3-MC, this QCC variation is explainable by the onset of the uniaxial rotation in the asymmetric potential wells as mentioned in 5.1.A. A quite sharp component of the ^{2}H spectra observed at temperatures above 400 K, is provably assignable to decomposed cations, because the existence of organic radicals, which seems to be produced by decomposition of the tetramethylenediammonium ions, was confirmed by ESR measured at 298 K in C42-MC which had been once heated to 470 K.

^1H NMR spin-lattice relaxation time (T_1)

Recoveries of ^{1}H magnetization after 180°-τ-90° rf-pulse, $(M(\infty)-M(\tau))/M(\infty)$, observed at 54.3 MHz in C42-MC, are shown in Figure 5.D.3. At the lowest temperature of 106 K, the most part of the recovery curve except the extremely short τ component could be fitted by a single straight line as shown in Figure 5.D.3. In the temperature region above 150 K, the fast-recovering part could not be ignored, and the recovery was divided into two exponential components which had different time constants (T_1). In the middle and bottom graphs in Fig. 5.D.3, solid lines denote the slow-relaxing component with a long T_1, and the open circles stand for the fast-relaxing one with a short T_1 obtained by subtracting the contribution of the slow-relaxing one from the whole magnetization observed. With rise of temperature, the increase in the ratio of fast-relaxing component was seen in Figure 5.D.3.

The temperature dependence of the fraction of the short T_1 component is shown in Figure 5.D.4. With rising temperature, the short component fraction increased and went over 50 % around 220 K. Accordingly, it was clarified that the short T_1 component is major in the temperature region higher than 220 K.

The temperature dependence of ^{1}H NMR spin-lattice relaxation times observed in C42-MC is shown in Figure 5.D.5. In a temperature region from 100 to 200 K, T_1 values of the slow-relaxing component hardly varied and a shallow minimum could be observed around 300 K. Since the onset of the C_3 rotation of NH_3^+ groups below 140 K was predicted by the QCC analysis in C42d_6-MC, it is likely that the T_1 behavior at temperatures around 140 K is governed by this motion. However, the minimum value of

0.29 s observed in this region is much longer than 0.06 s of the minimum calculated for the NH_3^+ rotation. By referring to the T_1 analysis in C82-MC, it is provable that there is a distribution in the correlation time of the NH_3^+ motion. From the QCC analysis, the T_1 minimum around 300 K can be assigned to the cationic uniaxial rotation as a whole around its long axis. The minimum value of about 0.15 s is longer than 0.045 s calculated for this motion, explainable by the asymmetric potential well model suggested in the QCC analysis of C42d_6-MC. Therefore, the T_1 curve of the long T_1 component was fitted by using a following equation.

$$\frac{1}{T_1} = \frac{1}{T_1^{ASYM}} + \frac{1}{T_1^{DIS}},$$

where T_1^{ASYM} and T_1^{DIS} are already defined in 5.1.A and 4.1.A, respectively. The motional parameters determined by this fitting are shown in Table 5.D.1.

As for the fast-relaxation component, T_1 decreased monotonically with rising temperature, and gave quite short values less than 10 ms in the high temperature region above 300 K. This phenomenon is similar to the T_1 variation observed in C41-MC. The T_1 reduction to a few ms is, accordingly, provably explained by the excitation of cationic 2D diffusion giving a fluctuation in the interaction between ^1H spins and paramagnetic electron spins as stated in 5.1.C. No explicit minimum could be observed in the T_1 data of the fast-relaxing component, so only the activation energy in the cationic 2D diffusion was estimated by fitting Eq. (13) to these data.

Electrical conductivity

Temperature dependences of the product of electrical conductivity σ observed in C42-MC and temperature T were shown in Figure 5.D.6. Closed and open circles denote the ln (σT) observed in the first and the second run, respectively, in the same sample. In the first measurement, conductivity of $3.3*10^{-6}$ Sm^{-1} was obtained at 325 K. With rise of temperature, ln (σT) increased linearly. Around 450 K, the increasing rate of ln (σT) became steeper and conductivity of $1.1*10^{-4}$ Sm^{-1} was obtained at 472 K. This behavior was also seen in the second measurement. The linear increase of ln (σT) implies the ionic conduction in C42-MC, so the excitation of 2D diffusion of tetramethylenediammonium ions is confirmed. The diffusional activation energy, E_a, was estimated by using Nernst-Einstein relation in the temperature region below 450 K where ln (σT) increases linearly. The obtained E_a values were 30±0.2 kJ mol^{-1} in the first measurement, and 36±0.2 kJ mol^{-1} in the second. These E_a values are larger than 15 kJ mol^{-1} obtained in the ^1H T_1 analysis. This is because the self-diffusion of short-range diffusional jumps of the order of 1 nm mainly contributes to the NMR relaxation, while the long range diffusion of 0.1-1 μm order can be obtained in the present ac conductivity measurement which is usually expected to give a higher activation energy. As for the change of slope around 450 K, a clear explanation cannot be given in this study, but it is likely that there exist two types of cations in C42-MC: one can diffuse easily, and the other not.

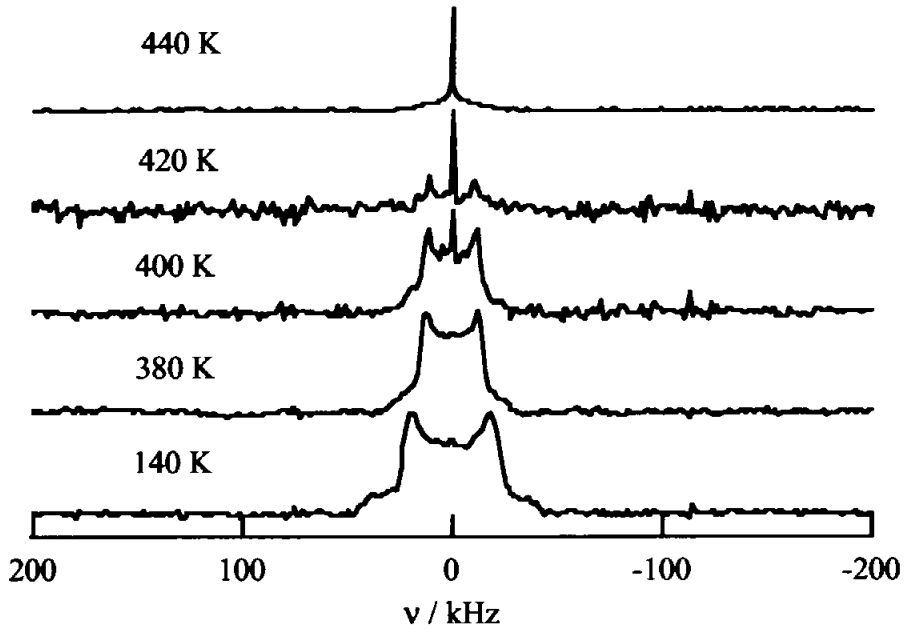

Fig. 5.D.1. ^{2}H NMR spectra observed in $ND_3(CH_2)_4ND_3$-tetrasilicicfluormica.

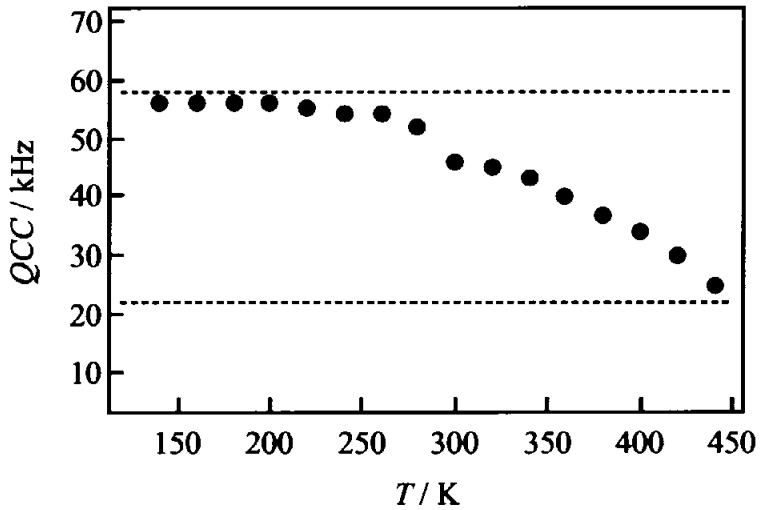

Fig. 5.D.2. The temperature dependence of quadrupole coupling constant (QCC) estimated from the linewidths of ^{2}H NMR spectra observed in $ND_3(CH_2)_4ND_3$-tetrasilicicfluormica. Broken lines stand for the calculated QCC for two motional modes of $ND_3^+(CH_2)_4ND_3^+$ ion: ND_3^+ rotation about its C_3 axis (top) and cationic uniaxial rotation as a whole about its long axis (bottom).

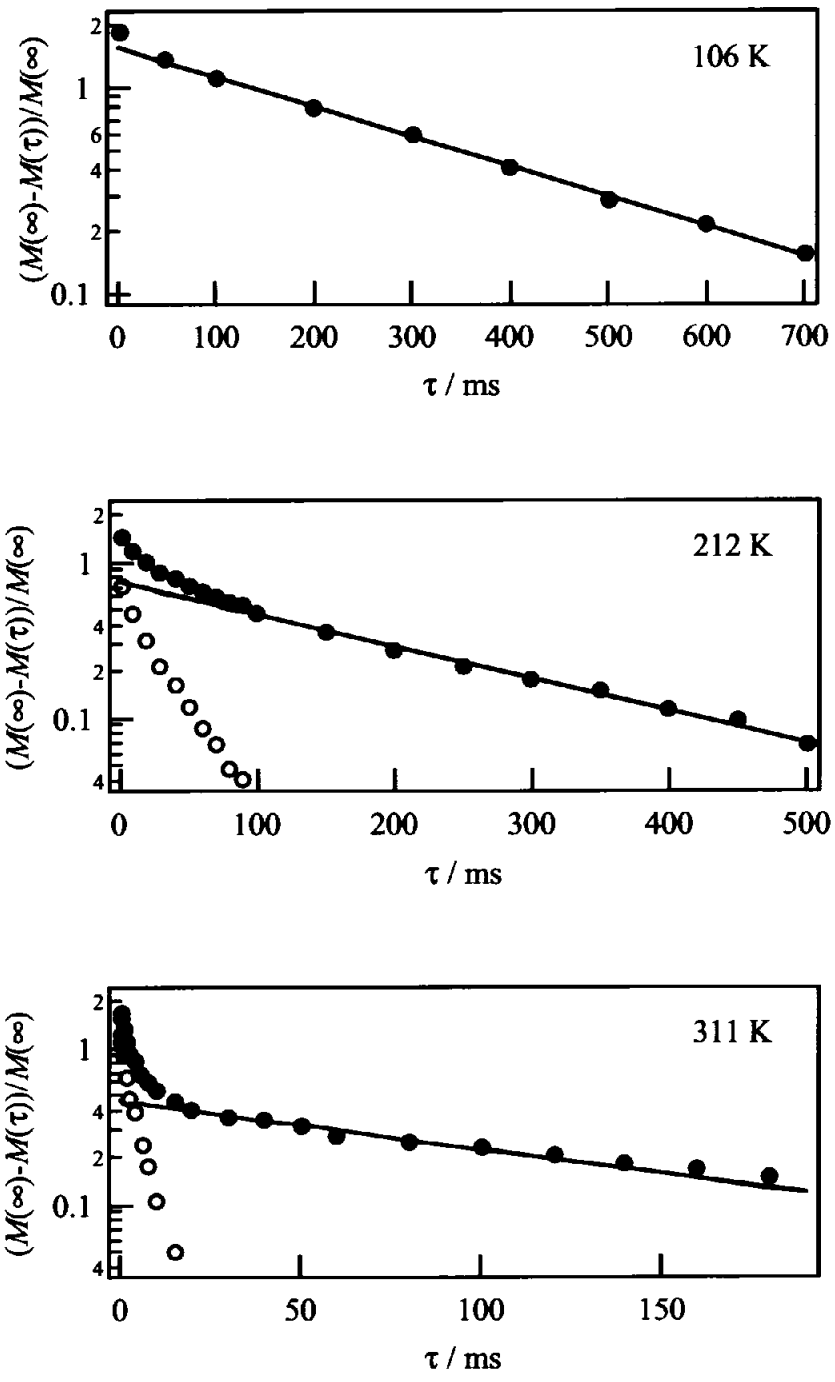

Fig. 5.D.3 Recoveries of ^{1}H magnetization (●) observed at a Larmor frequency of 54.3 MHz in $ND_3(CH_2)_4ND_3$-tetrasilicicfluormica. The slope of solid line affords the spin-lattice relaxation time (T_1) of the slow-relaxing component. The fast-relaxing component (○) is given as the difference between the observed magnetization and calculated values shown by the solid line.

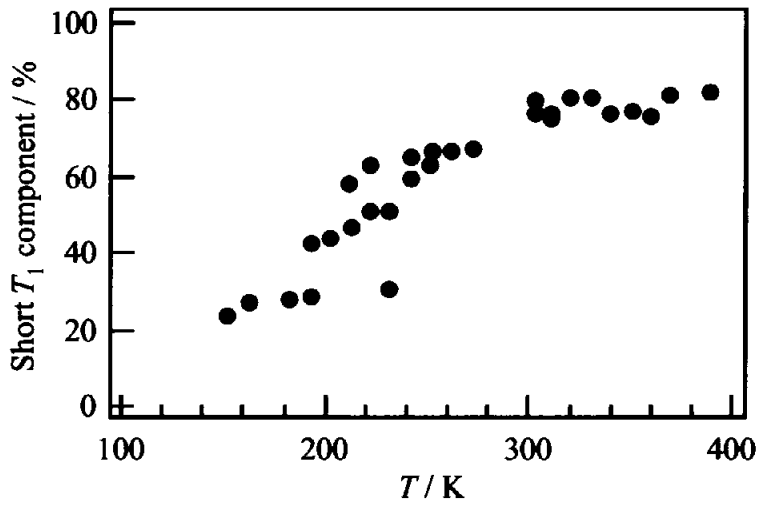

Fig. 5.D.4. The temperature dependence of the ratio of short T_1 component.

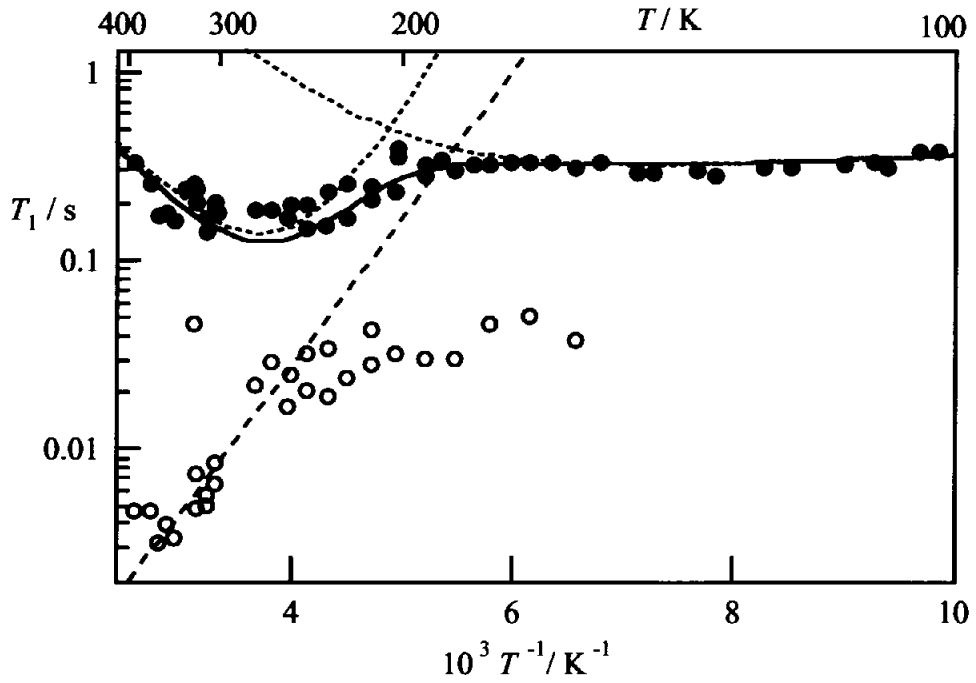

Fig. 5.D.5. ^1H NMR spin-lattice relaxation times T_1 observed at 54.3 MHz (●) in $NH_3(CH_2)_4NH_3$-tetrasilicicfluormica. Dotted lines stand for T_1 components calculated at 54.3 MHz, and their superposition is expressed by the solid line. Broken line depicts T_1 values calculated by introducing the paramagnetic interaction.

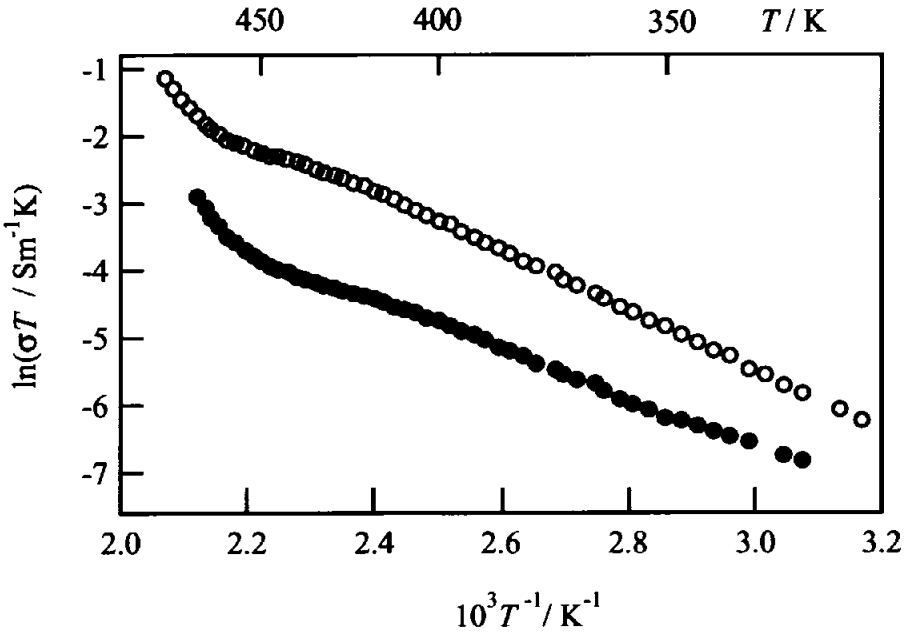

Fig. 5.D.6. The temperature dependence of electrical conductivity σ observed in $NH_3(CH_2)_4NH_3$-tetrasilicicfluormica by the two-terminal method at 1 kHz. Closed and open circles stand for the values obtained in the virgin sample and that once heated to 472 K, respectively.

Table 5.D.1. The fitting parameters determined by the analysis of ^1H NMR spin-lattice relaxation times observed in $NH_3(CH_2)_4NH_3$-tetrasilicicfluormica: motional modes, activation energies (E_a or $*E_{a1}$), reductions of second moment (ΔM_2) and a difference of asymmetric potential depths ($\Delta=E_{a1}-E_{a2}$). Calculated values of ΔM_2 are also shown in parentheses. *: the case of asymmetric potential model.

motional mode	$E_a(*E_{a1})$ / kJ mol^{-1}	ΔM_2	β	Δ
NH_3-rot	8.0	9.9(9.2)	0.06	-
uniaxial-rot	*18	*11(11)	-	*5
2D-diffusion	15	-	-	-

E. Guanidinium-Tetrasilicicfluormica (Gu-MC and Gud_6-MC)

^{2}H NMR spectra

^{2}H NMR spectra observed in Gud_6-MC are shown in Figure 5.E.1. In the temperature region below 180 K, wide spectra were obtained with a complicated structure at their centers. At 180 K a narrow spectrum component appeared clearly at the center of the wide component. In the temperature region above 180 K, only the narrow component could be observed. A bulge came out at the center of the spectra at 440 K.

The spectrum shape observed below 180 K is provably given at the beginning of the onset of a certain motional mode of guanidinium ions. The line shapes observed at 180 K and above 180 K are explainable by this cationic motion just before and in the motional narrowing state. A bulge observed at 440 K implies a further excitation of another motional mode of guanidinium ions.

Quadrupole coupling constants (QCC) estimated from linewidths of the main spectrum component are shown in Figure 5.E.2. In the temperature range below 180 K, QCC of 230±10 kHz was obtained. This value is a little larger than 200.5 kHz obtained in the rigid lattice of guanidinim-d_6 chloride [12], implying that guanidinium ions in the interlayer space of tetrasilicicfluormica are in the rigid state in the region below 180 K. Above 180 K, a QCC of 115±5 kHz was given. Since this value coincides with 115 kHz calculated for the cationic rotation about its C_3 axis by assuming the rigid lattice value to be 230 kHz obtained in Gud_6-MC in the temperature region below 180 K, the onset of

cationic C_3 rotation [C_3-rot] is expected in the temperature region above 180 K. The bulge observed at 440 K is explainable by the excitation of a motion of an amplitude larger than [C_3-rot], such as the tumbling of C_3 axis in addition to [C_3-rot].

^1H NMR spin-lattice relaxation time (T_1)

Recoveries of ^{1}H magnetization, $(M(\infty)-M(\tau)) / M(\infty)$, observed at 54.3 MHz are shown Figure 5.E.3. Except for the very small fast-recovering part, the most part of the recovery observed at 111 K could be fitted by a straight line decreasing with a characteristic time constant, T_1, In the temperature range higher than ca. 200 K, recovery curves could be divided to two straight lines with different T_1 values, as shown in the middle and bottom graphs in Fig. 5.E.3 where solid lines denote the slow-relaxing component with a long T_1, and open circles exhibit the fast-relaxing component given by subtraction of the long T_1 component from the observed whole magnetization. The temperature dependence of the fraction of the short T_1 component is shown in Figure 5.E.4. In the temperature region below 300 K, the fraction was about 30 %. It increased above 300 K, and exceeded 50 % at 360 K, indicating that the short T_1 component is major above 360 K.

Temperature dependences of ^{1}H NMR spin-lattice relaxation times measured in Gu-MC are shown in Figure 5.E.5. An explicit T_1 minimum at respective frequencies was observed around 220 K. By referring to the result of ^{2}H QCC in Gud_6-MC, it is reasonable that the minimum around 220 K is attributed to the cationic C_3 rotation. It is provable that there is little distribution in the motional correlation time because of the

sudden QCC reduction observed around 180 K. Hence, the minimum around 220 K was fitted by a simple BPP type theoretical curve written by Eq. (8). Obtained motional parameters are shown in Table 5.E.1. In the high temperature region above 350 K, T_1 was reduced in both long and short T_1 components, and went down to a few tens ms in the long component and a few ms in the short T_1 components around 430 K. The apparent frequency dependence was observed in the short T_1 component, which was major in this region, but not in the long T_1 component. From the analogy to T_1 analysis in C41-MC and C42-MC, the T_1 reduction of the short T_1 component is assignable to the onset of 2D diffusion of guanidinium ions from considering the electron paramagnetic interaction, so the T_1 data of this component were fitted by using Eq. (13). The determined activation energy for the cationic 2D diffusion is also shown in Table. 5.E.1. As for the long T_1 component, another relaxation mechanism should be considered. It is known that nuclei apart from paramagnetic spins relax through the mechanism called spin diffusion [10]. Spin diffusion makes remote nuclei relax by carrying the lattice temperature dispensed by electronic spins through the mutual flips between neighboring nuclear spins. If the relaxation is governed by the direct interaction between electronic spins and nuclear spins, T_1 varies in proportion to ω_I^2 in the low temperature region where $\omega_I\tau \gg 1$. On the other hand, in the spin diffusion limited case, T_1 is proportioned to $\omega_I^{1/2}$ in the same region [10]. In short, the frequency dependence of T_1 in the low temperature region in the former case is larger than that in the latter. Since T_1 values of the long T_1 component are almost in proportion to $\omega_I^{1/2}$, it is likely that the spin diffusion is the dominant mechanism of relaxation of the long T_1 component.

Electrical conductivity

The temperature dependences of electrical conductivity, σ, observed in Gu-MC are shown in Figure 5.E.6. Closed and open circles denote the conductivities in the first and second measurements, respectively, in the identical sample. In the first measurement, the conductivity could be observed from 430 K upon heating, and it increased with the rise of temperature. In the second measurement, almost the same result as in the first was obtained. So, the structure of the intercalated guanidinium ions in the interlayer space is expected not to be changed by the heating treatment. In both measurements, a linear increase of ln (σT), which is characteristic of the ionic conduction, was observed, so the onset of cationic diffusion was confirmed. The activation energies of 63±1 and 52±1 kJ mol^{-1} for this mode were determined from the slops of ln (σT) variations in the first and second measurements, respectively. These E_a values are larger than 25 kJ mol^{-1} estimated in the ^{1}H T_1 analysis for the same mode. This difference seems to come from different time scales of the cationic diffusion in NMR and electronic conductivity measurement as mentioned in 5.1.D.

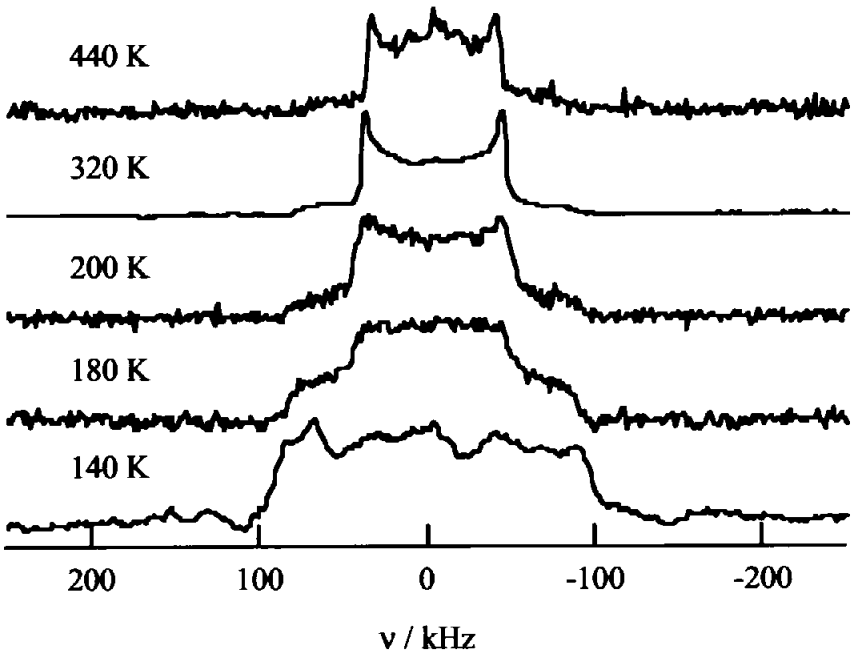

Fig. 5.E.1. ^{2}H NMR spectra observed in $C(ND_2)_3$-tetrasilicicfluormica.

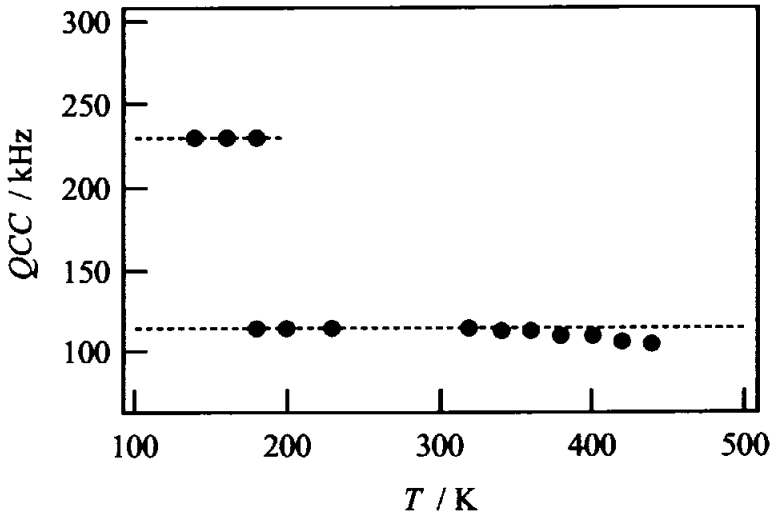

Fig. 5.E.2. The temperature dependence of quadrupole coupling constants (QCC) estimated from the linewidths of ^{2}H NMR spectra observed in $C(ND_2)_3$-tetrasilicicfluormica. The lower broken line stand for the calculated QCC for the cationic rotation about its C_3 axis of $C(ND_2)_3^+$ ion by assuming the rigid lattice value to be 230 kHz exhibited by a upper broken line.

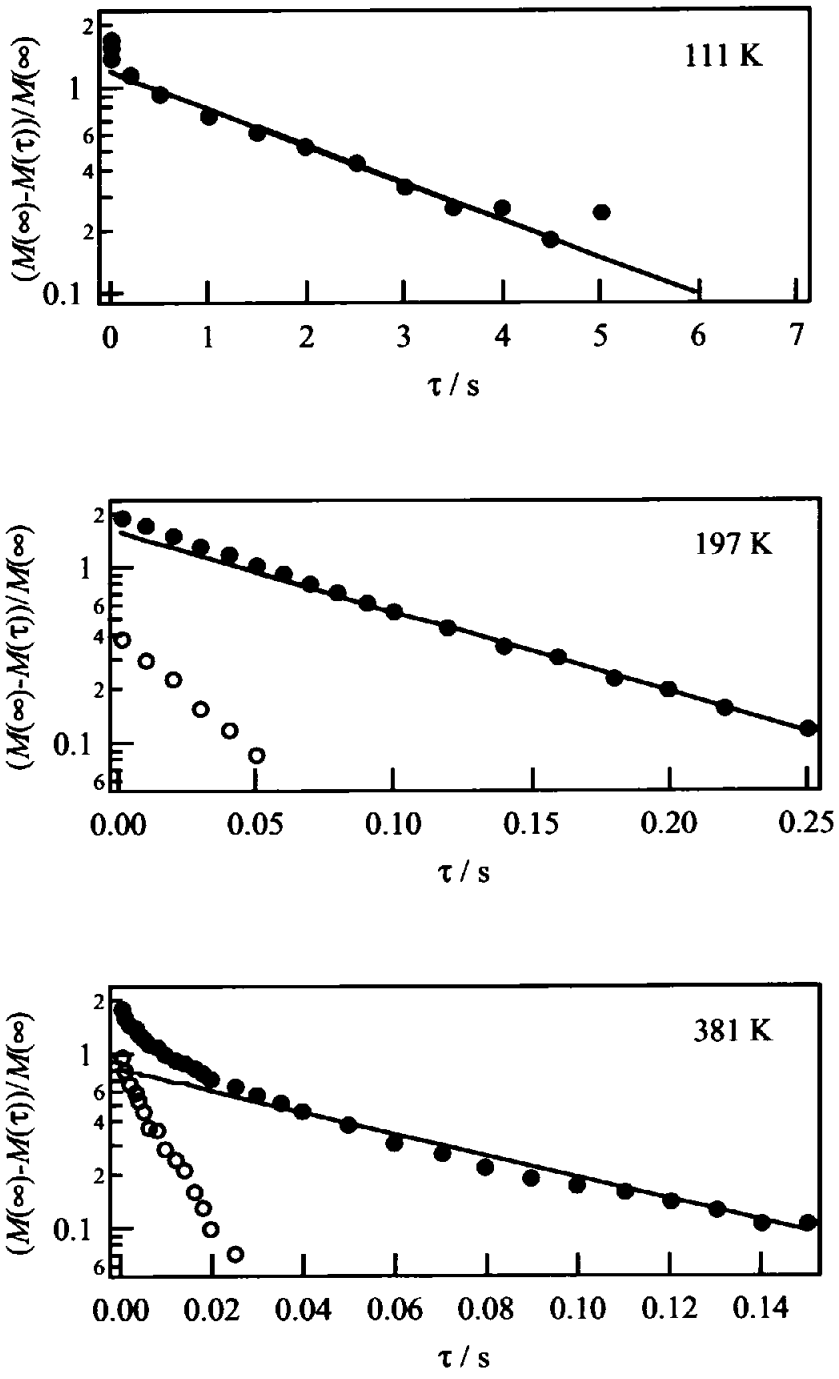

Fig. 5.E.3. Recoveries of ^{1}H magnetization (●) observed at a Larmor frequency of 54.3 MHz in $C(NH_2)_3$-tetrasilicicfluormica. The slope of solid line affords the spin-lattice relaxation time (T_1) of the slow-relaxing component. The fast-relaxing component (○) is given by the difference between the observed magnetization and the solid line.

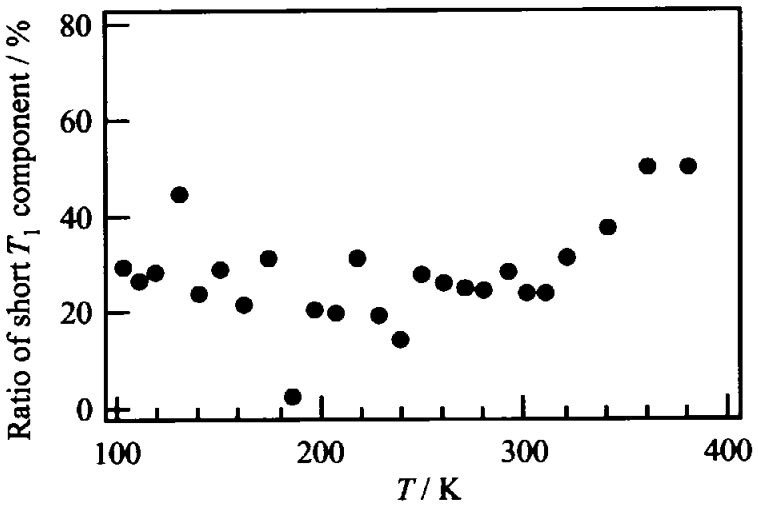

Fig. 5.E.4. The temperature dependence of the ratio of short T_1 component.

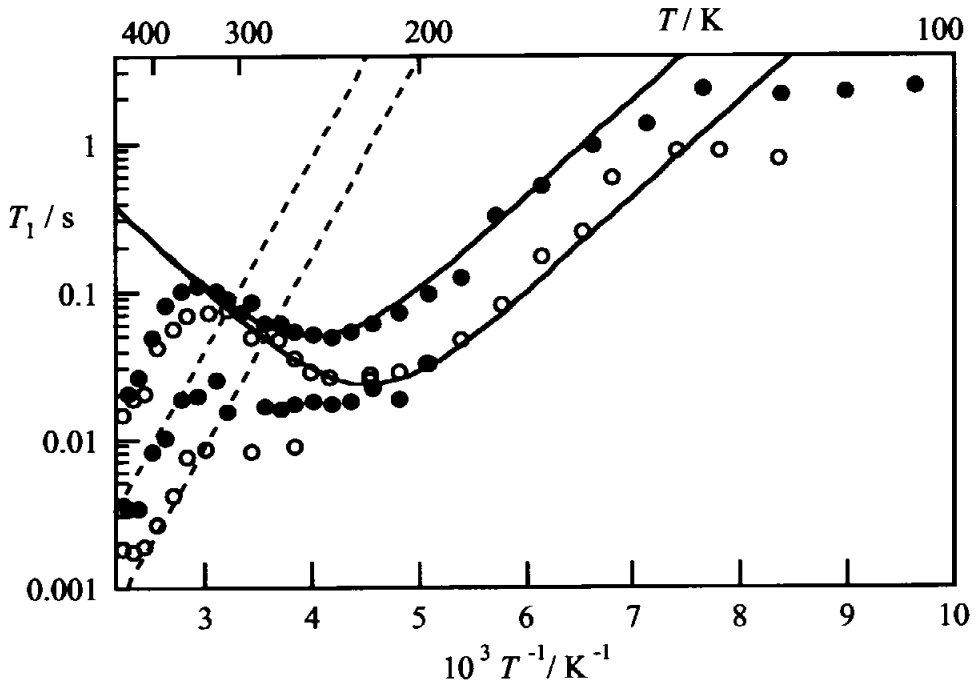

Fig. 5.E.5. ^{1}H NMR spin-lattice relaxation times T_1 observed at 54.3 MHz (●) and 26.7 MHz (○) in $C(NH_2)_3$-tetrasilicicfluormica. Solid lines denote T_1 values calculated at 54.3 and 25.6 MHz. A broken line stands for T_1 values calculated by introducing paramagnetic interaction.

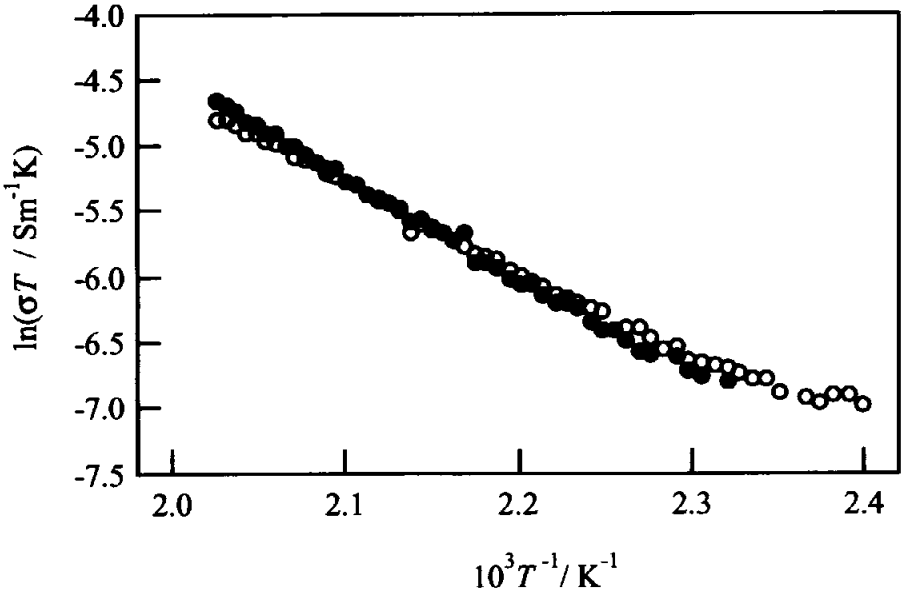

Fig. 5.E.6. The temperature dependence of electrical conductivity σ observed in $C(NH_2)_3$-tetrasilicicfluormica by the three-terminal method at 1 kHz. Closed and open circles stand for the values obtained in the first measurement and the second in the same sample.

Table 5.E.1. The fitting parameters determined in the analysis of ^1H NMR spin-lattice relaxation times observed in $C(NH_2)_3$-tetrasilicicfluormica: motional modes, activation energies (E_a), a reduction of second moment (ΔM_2). A calculated value of ΔM_2 is shown in parentheses.

Motional mode	E_a / kJ mol^{-1}	ΔM_2
C_3-rot	12	9.9(12)
2D-diffusion	25	-

F. Trimethylammonium-Tetrasilicicfluormica (M3-MC, M3*d*-MC)

^2H NMR spectra

^2H NMR spectra observed in M3*d*-MC are shown in Figure 5.F.1. No marked temperature dependence was observed in both lineshape and linewidth. Quadrupole coupling constants (QCC) estimated from the linewidths of all ^2H spectra in Fig 5.F.1 were approximately 155±5 kHz. These values are close to 173 kHz observed in the rigid state of an ND_3^+ group in ethylammonium chloride [8]. The difference between 155 kHz and 173 kHz can be explained by the onset of the tumbling of the cationic C_3 axis. Therefore, it is revealed that large amplitude motions of trimethylammonium ions such as the overall rotation are not excited in M3*d*-MC even at 440 K.

Electrical conductivity

Temperature dependences of electrical conductivities, σ, observed in M3-MC are shown in Figure 5.F.2. Closed and open circles stand for conductivities in the first and the second measurements, respectively, using the same sample tablet.

In the first measurement, the conductivity could be determined from room temperature, and increased with the rise of temperature. Around 430 K, the slope of the temperature dependence of conductivity became steep, and σ of $2.4*10^{-4}$ S m^{-1} was obtained at 498 K. A linear increase of ln (σT) plotted against T^{-1} was seen between 300 and 430 K and between 430 and 494 K, indicating the ionic conduction, that is, the onset of the cationic diffusion in M3-MC. The change in the slope of the conductivity

means that there are two kinds of trimethylammonium ions with different mobilities for cationic diffusion in the interlayer space of tetrasilicicfluormica. By using the Nernst-Einstein relation, activation energies of cationic diffusion were determined from slopes of ln (σT) vs. T^{-1} plots to be 12±1 and 89±2 kJ mol^{-1} between 300 and 430 K and between 430 and 494 K, respectively.

In the second measurement, the conductivity was higher than in the first by the order of 10^1 in the whole temperature range. The explicit change of temperature coefficient of the conductivity could not be seen. These phenomena provably indicate that the rearrangement of the trimethylammonium ions occurs by the thermal treatment in the first measurement, and circumstances around intercalated cations become more homogeneous than in the unheated virgin sample.

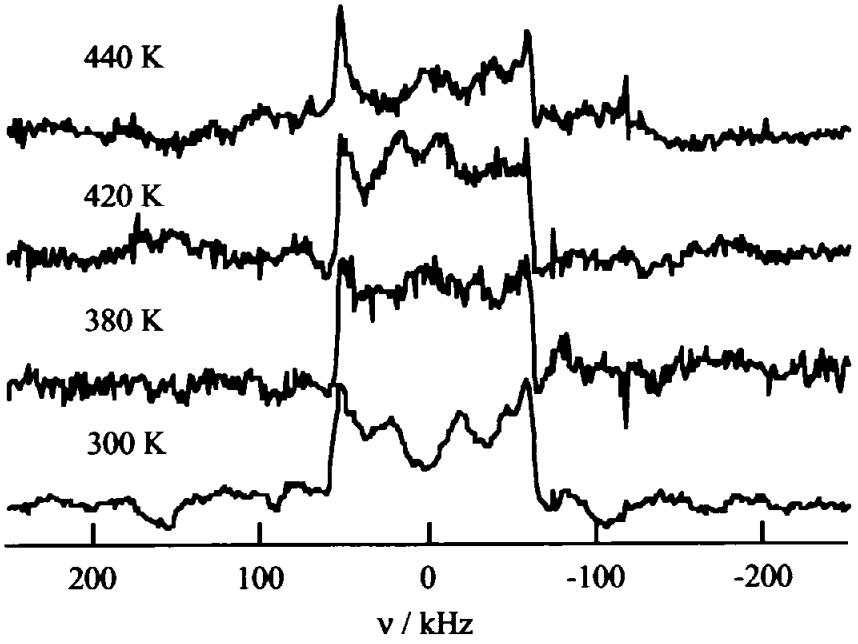

Fig. 5.F.1. ^{2}H NMR spectra observed in $N(CH_2)_3D$-tetrasilicicfluormica.

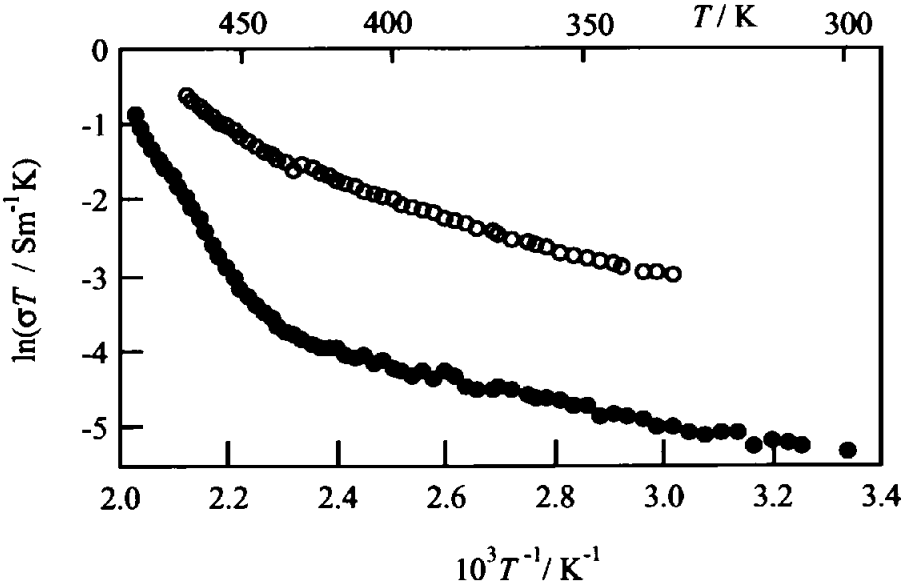

Fig. 5.F.2. The temperature dependence of electrical conductivity σ observed in $NH(CH_3)_3$-tetrasilicicfluormica by the two-terminal method at 1 kHz. Closed and open circles stand for values obtained in the first measurement and the second in the identical sample.

G. Tetramethylammonium-Tetrasilicicfluormica (M4-MC)

^1H NMR spin-lattice relaxation time (T_1)

Recovery curves of magnetization in M4-MC, $(M(\infty)-M(\tau))$ / $M(\infty)$, after a 180° rf-pulse in the ^1H NMR spin-lattice relaxation time measurement are shown in Figure 5.G.1. Closed circles represent observed magnetization values. In the low temperature region below 197 K, magnetization curves could be divided into two T_1 components as shown in the upper graph in Fig. 5.G.1, where the slow-relaxing component with a long T_1 is depicted by a solid line and the fast-relaxing one, which was given by the difference between the total magnetization and the contribution from the long T_1 component, is drawn by open circles. At 197 K (see the middle graph in Fig. 5.G.1), the recovery curve was reproduced by a straight line. In the high temperature region above 197 K, recovery curves again consist of two relaxing components as seen in the lower graph where the same notations are used as in the upper graph. The ratio of the short component to the whole magnetization is shown in Figure 5.G.2. Around 100 K, the short and the long T_1 components were almost same, indicating that there exist nearly the same amount of two kinds of tetramethylammonium ions in different circumstances. The decrease of the short component was observed up to 170 K, which provably implies that the circumstance around protons characterized by the short T_1 turns to that around protons with a long T_1. However, no detailed origins in the difference between short and long components below 197 K could be specified in this study. In the temperature range above 197 K, the short T_1 component was again

increased with rising temperature and exceeded 50 % above 400 K. This change means that protons of fast-relaxation increase above 197 K and become the majority in M4-MC above 400 K.

The temperature dependence of ^{1}H NMR spin-lattice relaxation time (T_1) is shown in Figure 5.G.3. T_1 values of the short component varied parallel to those of the long one. The minima of both short and long T_1 components were observed around 200 K. Since the long T_1 component is major around 200 K, and the origin of the short T_1 component is not clarified in this temperature region, here, only the minimum of the long T_1 component will be discussed. The minimum of long T_1 component was fitted by a simple BPP type theoretical curve written by Eq. (8) because of its symmetric shape. The fitting parameters are shown in Table. 5.G.1. The obtained difference of the second moment, ΔM_2, between before and after the onset of the motion was 15 G^2. This value is close to 18.9 G^2 calculated for the simultaneous onset of the rotation of four methyl groups around their C_3 axes [19], indicating that this mode is excited below 200 K. In the high temperature region above 350 K, both T_1 values were reduced with temperature. At 448 K, T_1 values reached 0.035 and 0.008 s in the long and short T_1 components, respectively. These values are much shorter than 0.064 s calculated for the excitation of the cationic overall rotation. From the analogy to the analysis on Gu-MC, this T_1 behavior above 350 K is expected to be explainable by the interaction between ^{1}H and paramagnetic electron spins inside the clay. The reduction of the short T_1 component is attributed to the onset of cationic isotropic rotation together with 2D diffusion which cause fluctuation of the direct interaction between ^{1}H spins and electron spins, since a

few ms of T_1 is unlikely to be given thorough any other relaxation mechanisms. Since this T_1 component is major above 400 K, most of the tetramethylammonium ions perform 2D self-diffusion in the high temperature region and experience the fluctuation of paramagnetic field for the period of the motional correlation time. The T_1 data of short T_1 component was fitted by using Eq. (13), and the obtained activation energy for the 2D diffusion is shown in Table 5.G.1. By referring to the discussion in Gu-MC, it is likely that the T_1 variation of the long T_1 component is governed by the spin-diffusion through the neighboring ^1H spins.

Electrical conductivity

Temperature dependences of electrical conductivities (σ) observed in M4-MC are shown in Figure 5.G.4. Closed and open circles represent conductivities determined in the first and the second measurement, respectively, in the identical specimen.

In the first measurement, the conductivity was measured from 387 K. With rising temperature, the conductivity was increased and went up to $2.4*10^{-4}$ Sm^{-1} at 499 K. In two temperature ranges 387-450 K, and 450-500 K, a linear increase of In (σT) was observed, indicating the presence of ionic conduction. Thus, the onset of the cationic 2D diffusion predicted in ^1H T_1 was confirmed by this result. The fact that the slope of temperature dependence of conductivity is not uniform over the whole temperature region implies that the circumstances around tetramethylammonium ions are inhomogeneous in M4-MC. By using the Nernst-Einstein relation, activation energies for the 2D diffusion were estimated in the low and high temperature ranges to

be 30±0.5, and 95±3 kJ mol^{-1}, respectively. It is natural that these values are much larger than 16 kJ mol^{-1} determined by NMR measurement because of the difference in the time scale between electric conductivity and NMR measurements as mentioned in 5.1.F.

In the second measurement, the conductivity varied smoothly more than in the first measurement. Over the whole temperature region, σ values were higher than those obtained in the first measurement by the order of 10^1. From this result, it can be supposed that rearrangements of intercalated cations take place by the thermal treatment in the first measurement, and the circumstances around cations in the heated sample become more homogeneous and less restrained to the excitation of cationic 2D diffusion than in the virgin sample.

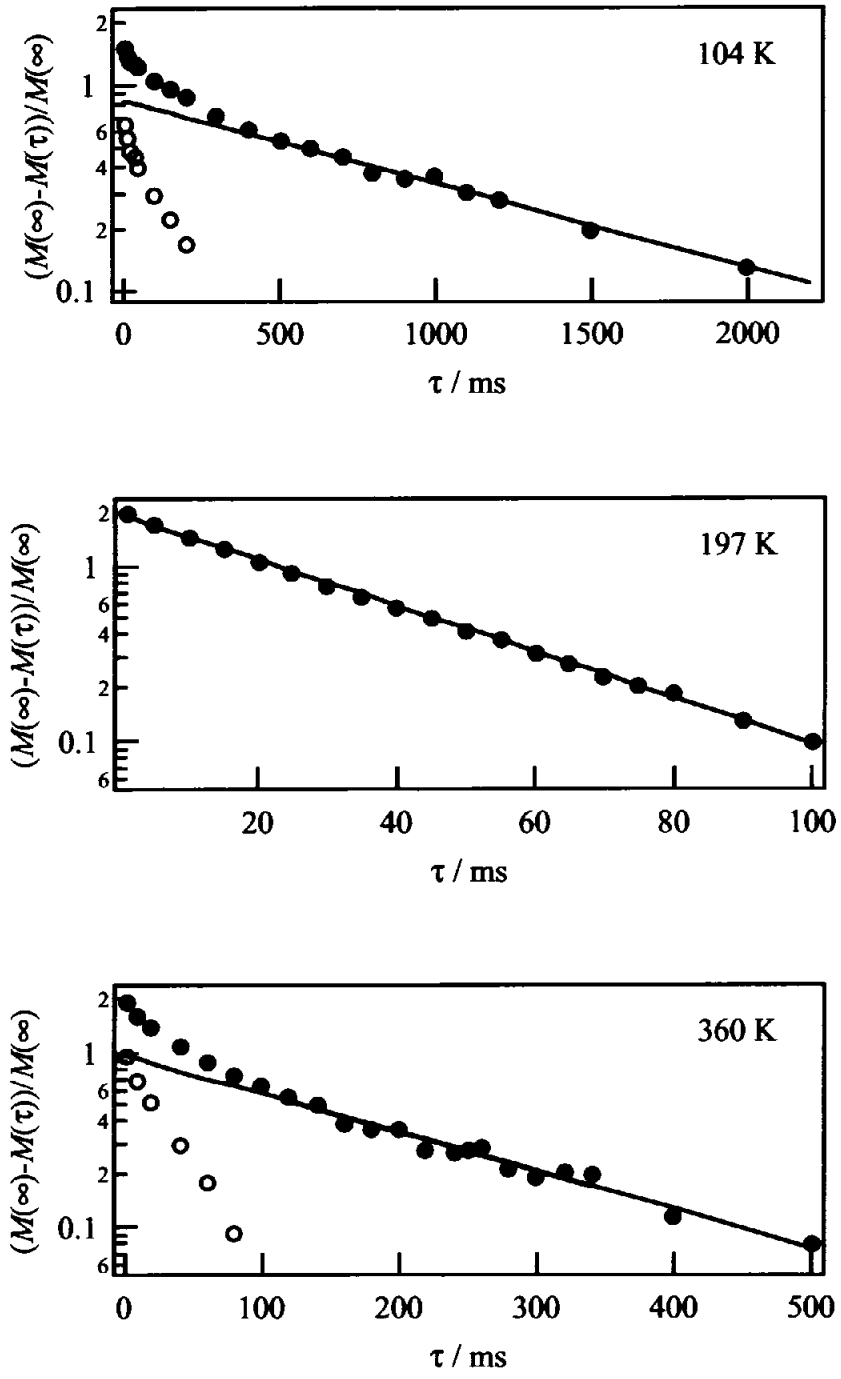

Fig. 5.G.1. Recoveries of ^1H magnetization (●) observed at a Larmor frequency of 54.3 MHz in $N(CH_3)_4$-tetrasilicicfluormica. The slope of solid line affords the spin-lattice relaxation time (T_1) of the slow-relaxing component. The fast-relaxing component (○) is given by the difference between the observed magnetization and the solid line.

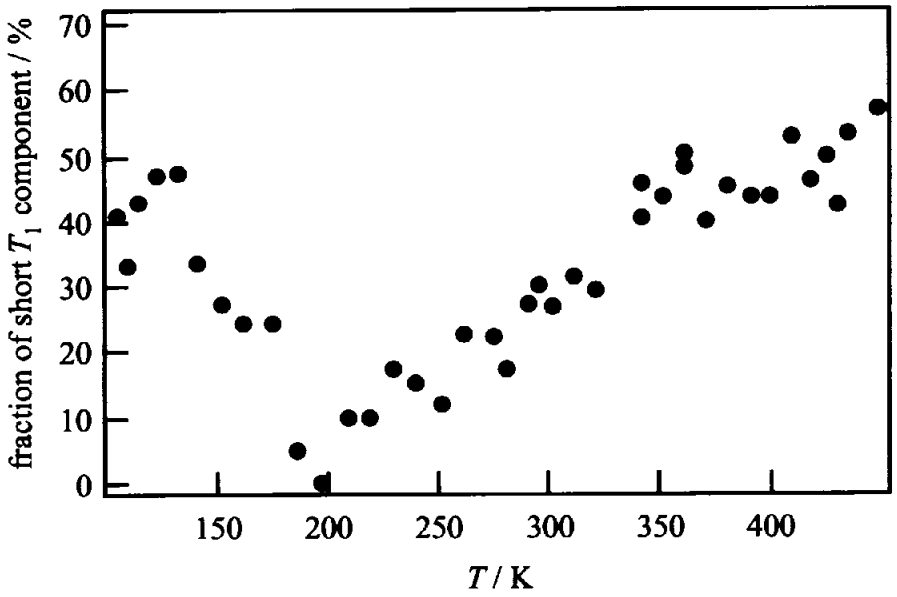

Fig. 5.G.2. The temperature dependence of the fraction of short T_1 component in $N(CH_3)_4$-tetrasilicicfluormica.

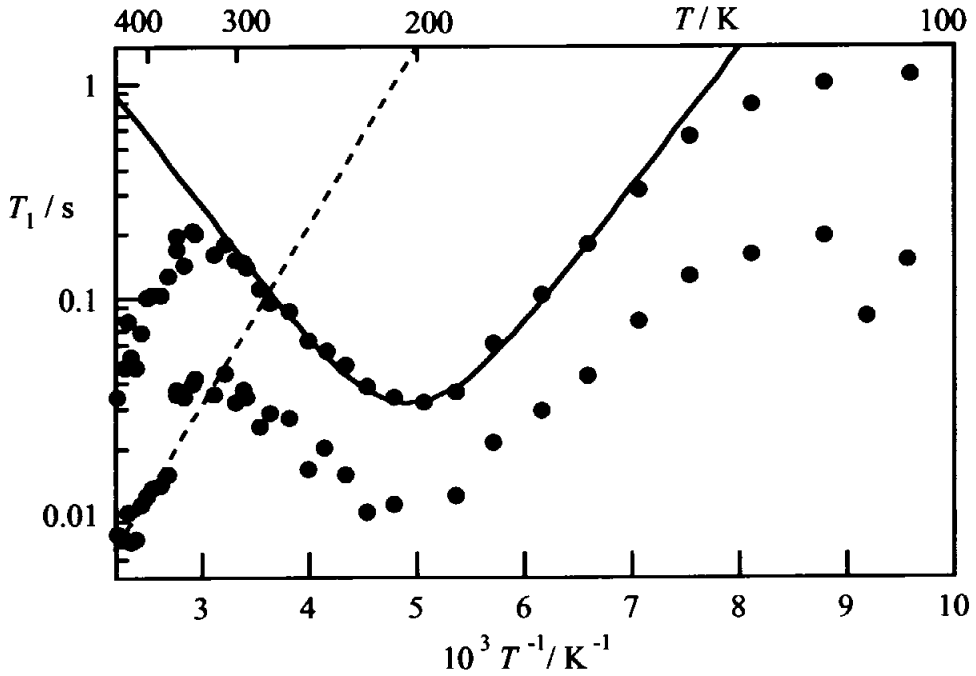

Fig. 5.G.3. ^1H NMR spin-lattice relaxation times T_1 observed at 54.3 MHz (●) in $N(CH_3)_4$-tetrasilicicfluormica. The solid line denotes T_1 values calculated at 54.3 MHz. The broken line stands for T_1 values calculated by introducing paramagnetic interactions.

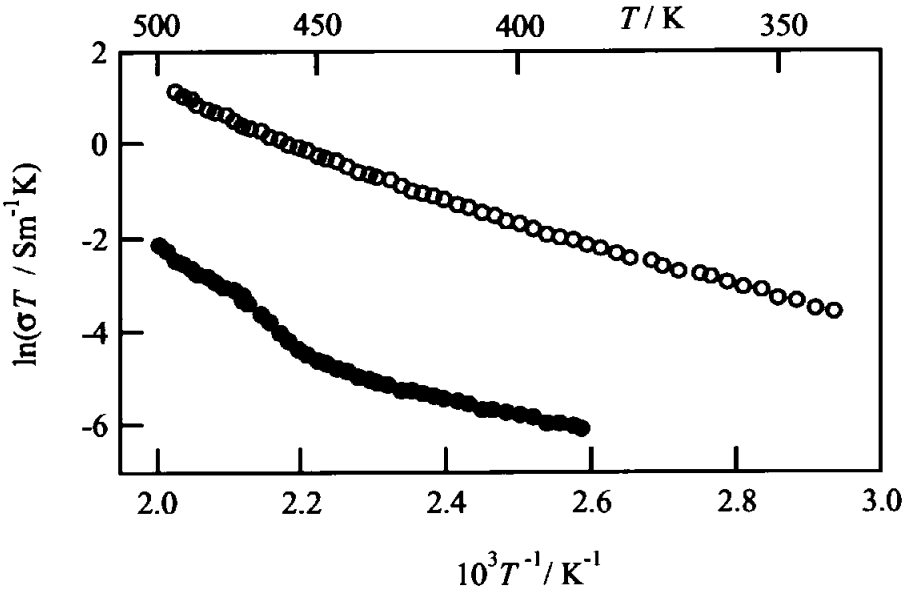

Fig. 5.G.4. The temperature dependence of electrical conductivity σ observed in $N(CH_3)_4$-tetrasilicicfluormica by the two-terminal method at 1 kHz. Closed and open circles stand for values obtained in the first measurement and the second in the same sample.

Table 5.G.1. Fitting parameters determined in the analysis of ^1H NMR spin-lattice relaxation times observed in $N(CH_3)_4$-tetrasilicicfluormica: motional modes, activation energies (E_a), and a reduction of second moment (ΔM_2).

motional mode	E_a / kJ mol^{-1}	ΔM_2
CH_3-rot	13	15
2D-diffusion	16	-

5.2 Conclusion

Dynamic properties of n-alkylammonium ions intercalated in tetrasilicicfluormica

As a new kind of 2D cationic motion, It was found the in-plane tumbling of *n*-octylammonium ions as a whole about axis perpendicular to the molecular axis in the high temperature range. The 2D space formed by clay sheets enables this new type of 2D motion, which could not so far be found in bulk crystals.

In the *n*-alkylammonium-tetrasilicicfluormica series, activation energies (E_a) for the NH_3^+ rotation of alkylammonium ions were shown to be much smaller than those in pure crystalline compounds, e.g., E_as of 5.5-8.0 kJ mol^{-1} are obtained in mica compounds as tabulated in Table 5.2.1, while, E_as are 23, 26.8, 28, 13.0 kJ mol^{-1} in $CH_3(CH_2)_3NH_3Br$ [13], $CH_3(CH_2)_3NH_3I$ [14], $CH_3(CH_2)_4NH_3Cl$ [20], and $CH_3(CH_2)_{11}NH_3Cl$ [15], respectively. These differences in the activation energies can be simply explained by the difference of electrostatic interactions in these two types of systems as given below: In mica layers, negative charges are dispersed over several oxygen atoms around the empty Mg site, so clay layers seem to attract NH_3^+ groups loosely more than the small size halide anions whose negative charges are located. Therefore, the activation barriers for the NH_3^+ rotation in tetrasilicicfluormica are expected to be smaller than those in the pure halide salts.

It is suggested in this study that the asymmetric potential well model can be adapted for the uniaxial rotation of alkylammonium ions in tetrasilicicfluormica. This result indicates that clay sheets contact closely with the whole alkylammonium ions, so

the subtle change of molecular orientation in the uniaxial rotation of alkylammonium ions alters potential energy of the vicinity of an intercalated cation. In such a situation, it is expected that the molecular size considerably affects the dynamic properties of intercalated cations. This effect can be seen in the activation energies of the uniaxial rotation. For example, the activation energies for the uniaxial rotation of short chain alkylammonium ions such as, *n*-butylammonium and tetramethylenediammonium ions, are 14 and 18 kJ mol^{-1}, respectively, and those of long chain ones (n=8), *n*-octylammonium and octamethylenediammonium ions are 23 and 40 kJ mol^{-1}.

Dynamic properties of plate-like guanidinium and trimethylammonium ions in tetrasilicicfluormica

Motional states of plate-like guanidinium and trimethylammonium ions in tetrasilicicfluormica are considerably distinct compared with those in pure 3D crystals. In Table 5.2.2, motional modes of guanidinium ions and activation energies so far determined in various 3D crystals and in Gu-MC are tabulated. Although the onset of the cationic C_3 rotation of guanidinium ions is observed in both 3D crystal and Gu-MC, the E_a observed in Gu-MC is much smaller than those in 3D crystals. This phenomenon can be attributed to the negative charges dispersed over the mica layers as mentioned above. Further more, it is notable that the 2D diffusion of guanidinium ions observed in Gu-MC is excited with keeping the orientation of the normal of the molecular plane perpendicular to the clay layer. In 3D crystals, the self-diffusion of guanidinium ions has been so far found only in the plastic phase of guanidinium perchlorate [23] where

the self-diffusion is always accompanied by the cationic isotropic rotation.

In the 2D diffusion of plate-like trimethylammonium ions in M3-MC, the normal of the molecular plane is also fixed and perpendicular to the clay sheets. On the other hand, the cationic self-diffusion is excited together with the cationic isotropic rotation in the 3D crystal such as $(CH_3)_3NHClO_4$ [21] and $(CH_3)_3NHBF_4$ [22].

Thus, the feature of the 2D diffusion of plate-like cations in the 2D space is the alignment of the molecular plane of intercalated ions. This characteristic motion is expected to originate from the Van der Waals affinity between mica layers and organocations, i.e., since the contact of mica layers with organocations stabilized the whole system of the intercalation compounds, plate-like cations tend to make their molecular plane be in contact with the clay layers.

2D diffusion in small organocations intercalated in tetrasilicicfluormica

It is remarkable that the excitations of the 2D diffusion of various small organocations, such as *n*-butylammonium, tetramethylenediammonium, guanidinium, trimethylammonium, and tetramethylammonium ions in the interlayer space of tetrasilicicfluormica were observed in this study, although there are not so many examples of bulk crystals in which the self-diffusion of the above cations is excited. The examples of the self-diffusion observed in bulk crystals, which contain the same cations employed in this study are shown in Table 5.2.3. The activation energies for cationic diffusion in the above mentioned intercalation compounds are considerably smaller than those in the bulk crystals consisting of the corresponding cations as shown in Table

5.2.3. Hence it can be concluded that the 2D diffusion of relatively small cations is easy to occur in the interlayer spaces in tetrasilicicfluormica. This phenomenon seems to be originated from the following properties of intercalation compounds of tetrasilicicfluormica. (1) there is much vacant space where intercalated small cations can move. (2) Because of the weak electrostatic attraction between tetrasilicicfluormica and intercalated cations, the activation barrier for cationic self-diffusion is relatively low. Therefore, the small cations can behave like 2D liquid or 2D gas in the interlayer spaces of tetrasilicicfluormica.

Table 5.2.1. Motional parameters determined in mica compounds in this study by ^1H NMR measurements: motional modes, activation energies (E_a or E_{a1}), parameters presenting width of τ distribution (β), and differences in asymmetric potential depths ($\Delta=E_{a1}-E_{a2}$). *: values estimated by adapting asymmetric potential model. **: values determined by the electric conductivity measurement.

compound	motional mode	$E_a(E_{a1}^*)$ / kJ mol^{-1}	β	Δ / kJ mol^{-1}
C81-MC	NH_3^+-rot	5.5	-	-
	CH_3-tumbling	5.9	-	-
	Uniaxial-rot	23*	-	5.0
C82-MC	NH_3^+-rot	6.0	0.3	-
	Chain-fluctuation	13	-	-
	Uniaxial-rot	40	-	-
C41-MC	CH_3-rot	5.7	-	-
	NH_3^+-rot	7.1	-	-
	Uniaxial-rot	14*	-	5.0
	2D-Diffusion	18 (short) 22 (long)	-	-
C42-MC	NH_3^+-rot	8.0	0.06	-
	Uniaxial-rot	18*	-	5.0
	2D-Diffusion	15	-	-
Gu-MC	C_3-rot	12	-	-
	2D-diffusion	25	-	-
M3-MC	2D-diffusion	12**, 89**		
M4-MC	CH_3-rot	13	-	-
	2D-diffusion	16	-	-

Tbale 5.2.2. Motional modes and activation energies (E_a) obtained in crystals of guanidinium salts and in $C(NH_2)_3$-tetrasilicicfluormica.

compound	motional mode	E_a / kJ mol^{-1}
$C(NH_2)_3X$ [12, 23] X=Cl, Br, I, NO_3, SCN	C_3-rot	50-78
$C(NH_2)_3MX_4$ [24] M=Au, Pt, Pd X=Cl, Br	C_3-rot	20-50
$C(NH_2)_3MX_6$[25] M=Pt, Sn, Te X=Cl	C_3-rot	52-57
$C(NH_2)_3ClO_4$ [23]	C_3-rot	39
	Isotropic rotation	10
	diffusion	41
Gu-MC	C_3-rot	12
	2D diffusion	25

Table 5.2.3. Examples of pure crystals with data on cationic self-diffusion and its activation energy (E_a).

cation	compound	E_a / kJ mol^{-1}
n-propylammonium	$CH_3(CH_2)_2NH_3Cl$[26]	41
n-butylammonium	$CH_3(CH_2)_3NH_3Cl$[27]	64
n-pentylammonium	$CH_3(CH_2)_4NH_3Cl$[20]	50
guanidinium	$(CH_3)_3NHClO_4$[21]	58
trimethylammonium	$(CH_3)_3NHBF_4$[22]	21
tetramethylammonium	$(CH_3)_4SCN$[28]	106